

# Chapter 3

## Experimental Shear Beam

By studying the effects of damage on the dynamic behavior of small-scale structures, one can form a better understanding of the effects of damage on actual buildings, thus aiding in the development of damage detection methods for large-scale structures. To this end, the effect of damage on the dynamic response of a civil structure is investigated experimentally using a small-scale (0.75 meter tall) shear beam. Damage is introduced into the shear beam by loosening the bolts connecting the columns to the floor, and a shake table is used to apply a consistent pulse at the base of the beam. The structural response is analyzed in both the time and frequency domains. The introduction of damage results in predictable changes in vertical shear wave propagation within the beam, as well as the surprising presence of repeating short-duration high-frequency signals that are presumably due to mechanical slippage and impact at the damaged floor.

The shear beam used in this study does not serve as a representative small-scale version of a real building, but rather serves as a mechanical system to which a damage detection method can be applied for establishing proof of concept. In fact, the shear beam used in this study is much stiffer than a typical full-scale five-story building. In tall buildings, a phenomenon known as the P- $\Delta$  effect can occur when the building undergoes a significant amount of lateral displacement, while considering the effects of gravity. The lateral movement of a story mass to a deformed position generates second-order overturning moments that are equal to the sum of the story weights P times the lateral displacements  $\Delta$  (Wilson, 2004). The contribution to moment from the lateral force is equal to the force times the story height.

Such a phenomenon cannot occur in the test specimen.

It is also worth mentioning that various sampling rates were used in the experiments, depending on the objectives. When the experimental objective is to determine the modal characteristics of the system, a lower sampling rate is used to record a longer segment of data. When the objective is to capture the high-frequency signals emitted by the damage events, a higher sampling rate, typically of 1 or 5 ksps but sometimes as high as 150 ksps, is used at the expense of recording a shorter segment of data. This is analogous to the strategy used in the continuous vibration monitoring of actual structures. Typically a lower sampling rate is used during ambient loading conditions, and a higher sampling rate is used in the event of an earthquake. As we will see in later chapters from the analysis of data recorded in existing full-scale structures *in situ*, a sampling rate of 100 sps seems to be high enough to detect high-frequency signals originating from structural damage events. For the structure used in this chapter, ‘high-frequency’ seismograms refers to signals of frequencies above 25 Hz, the fifth modal frequency of the structure.

### 3.1 Experimental Setup and Method

The five-story aluminum structure is fixed at its base to a shake table, as shown in the experimental setup in Figure 3.1. A high-sensitivity low-mass piezoelectric accelerometer is attached at each floor. Each accelerometer is connected to a data acquisition system and data logger (laptop computer). A list of the equipment and their specification sheets can be found in the Appendix. The dimensions of the structure can be found in Figure 3.2.

The shake table is used to supply a consistent pulse at the base of the shear beam that excites the structure over a broad range of frequencies. By using a repeatable source, differences in the dynamic response of the structure between trials due to differences in the source are minimized, and the effect of damage on the dynamic response of the structure can be more readily analyzed. As is apparent from Figure 3.3, the modal response of the structure is highly consistent between trials, though the introduction of damage results in the presence of transient signals that generally originate at the damaged floor. These transient

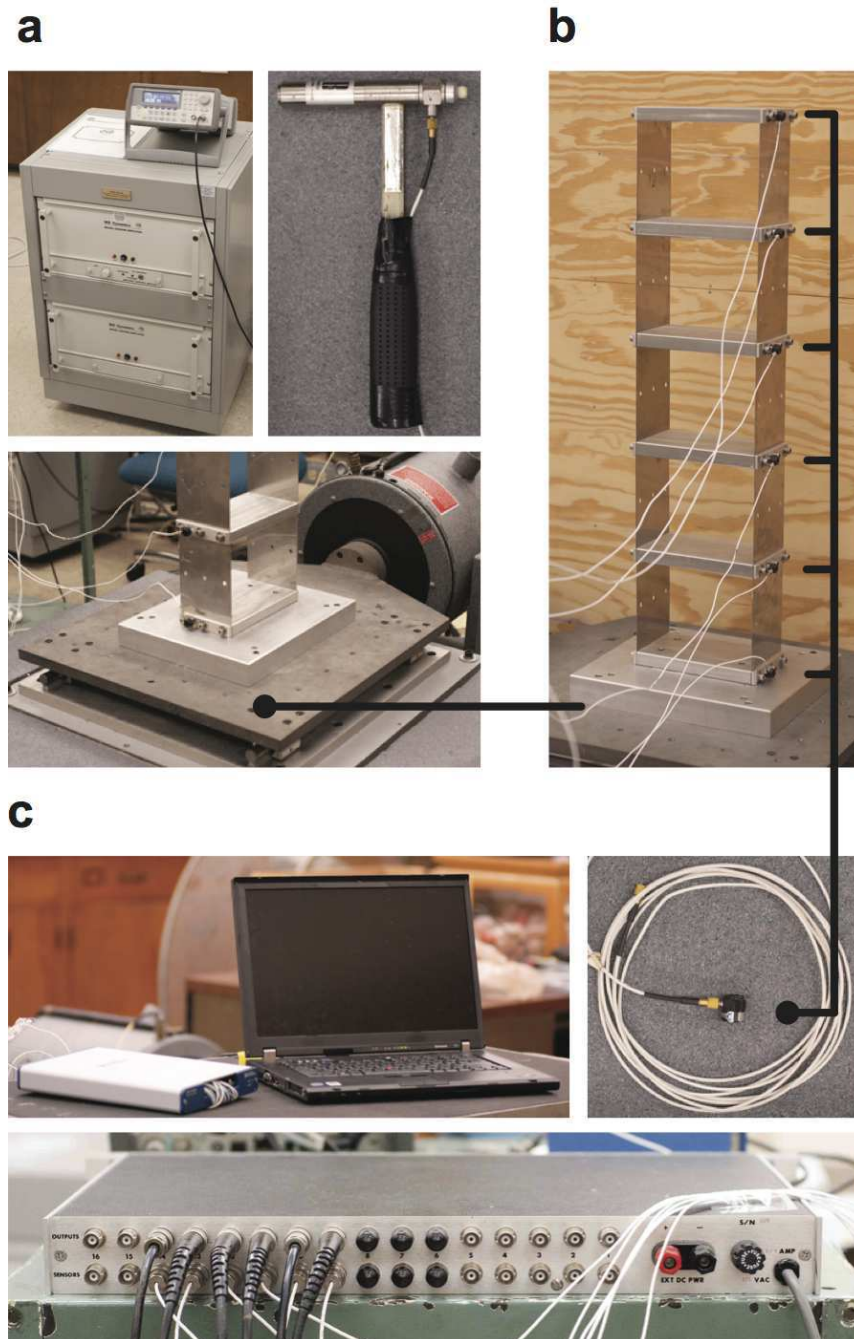


Figure 3.1: **Uniform Shear Beam Experimental Setup.** **a**, Input sources include an impulse hammer and a shake table. A signal generator and power amplifier are used in conjunction with the shake table to supply a consistent pulse at the base of the shear beam. **b**, The aluminum shear beam is firmly attached at its base to a shake table and is instrumented via an accelerometer attached to each of the five floors as well as the base. **c**, The low-mass piezoelectric accelerometers are connected to a power supply and signal conditioner, and a data acquisition device and laptop are used to record and store the data.

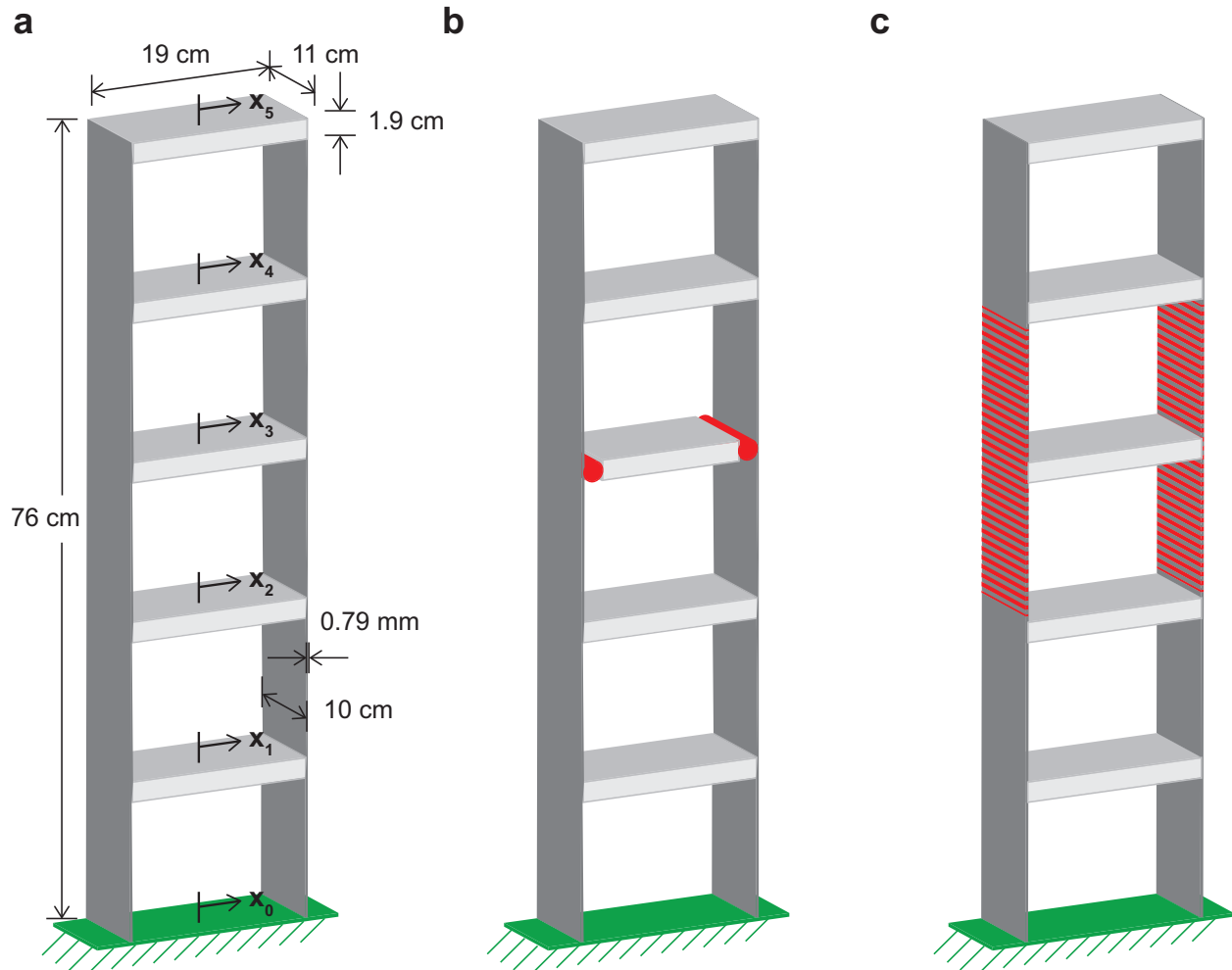


Figure 3.2: **Uniform Shear Beam Models.** **a**, The shear beam consists of two columns and six masses. Each column is constructed from five rectangular aluminum plates that are firmly connected to each floor by three screws per column. The masses are solid rectangular prisms. The shear beam is firmly screwed into a shake table. The bottom mass is screwed into the shake table platform, and thus is not accounted for in the five-degree-of-freedom model. Damage is introduced by loosening the screws connecting the columns to a floor mass. To model damage, two different frameworks are considered: damage to the connection and damage to the columns. **b**, In Damage Model I, the undamaged moment connection is replaced by a semi-rigid connection. **c**, In Damage Model II, the undamaged columns above and below the damaged floor are replaced by columns with reduced stiffness. In Damage Levels 1, 2, and 3, damage is introduced to the shear beam by incrementally loosening the 6 screws attaching the 2 columns to one of the five floors. Damage Level 1, 2, and 3 corresponds to a 1/6, 2/6, and 3/6 turn of each screw at the damaged floor, respectively. The amount of space created by loosening the screws is very small. The length of the gap created on one side is equal to 0.21 mm (0.0083"), 0.42 mm (0.017"), and 0.64 mm (0.025") for Damage Levels 1, 2, and 3, respectively.

signals are clearly observed over the modal response of the structure, and are presumably caused by mechanical slippage and impact at the loosened connections.

Structural damage is introduced into the shear beam by loosening the six screws attaching the two vertical the columns to a floor, shown in Figure 3.2, have been loosened. Three levels of damage are created by incrementally loosening the screws at the damaged floor. Damage levels one, two, and three correspond to a rotation of each screw by  $1/6$  turns ( $60^\circ$ ),  $2/6$  turns ( $120^\circ$ ), and  $3/6$  turns ( $180^\circ$ ), respectively. The type of screw used is a  $1/4$ -20 screw, which has 20 turns in one inch. The amount of space created by loosening the screws is very small. The length of the gap created on one side is equal to 0.21 mm (0.0083"), 0.42 mm (0.017"), and 0.64 mm (0.025") for Damage Levels 1, 2, and 3, respectively. By introducing damage incrementally, it is possible to study changes in the behavior of the small-scale structure for a progression of damage.

## 3.2 Theoretical Model:

### Linear Multi-Degree of Freedom System

The frame is modeled as a linear, uniaxial, five-degree of freedom system. Each floor in the model is constrained to displace along the horizontal x-axis; the vertical displacement and rotation of each floor is neglected. Masses are lumped at each floor and accounted for in the M matrix, columns contribute to the K matrix via their lateral stiffness, and either proportional or modal damping C is considered. The differential equations of motion for the model are given by:

$$M\ddot{x}(t) + C\dot{x}(t) + Kx(t) = f(t). \quad (3.1)$$

Let the displacement at the  $n^{th}$  floor be denoted by  $x_n(t)$ , the displacement at the ground be denoted by  $x_0(t)$ , and the external force applied to the  $n^{th}$  floor be denoted by  $f_n(t)$ . Then

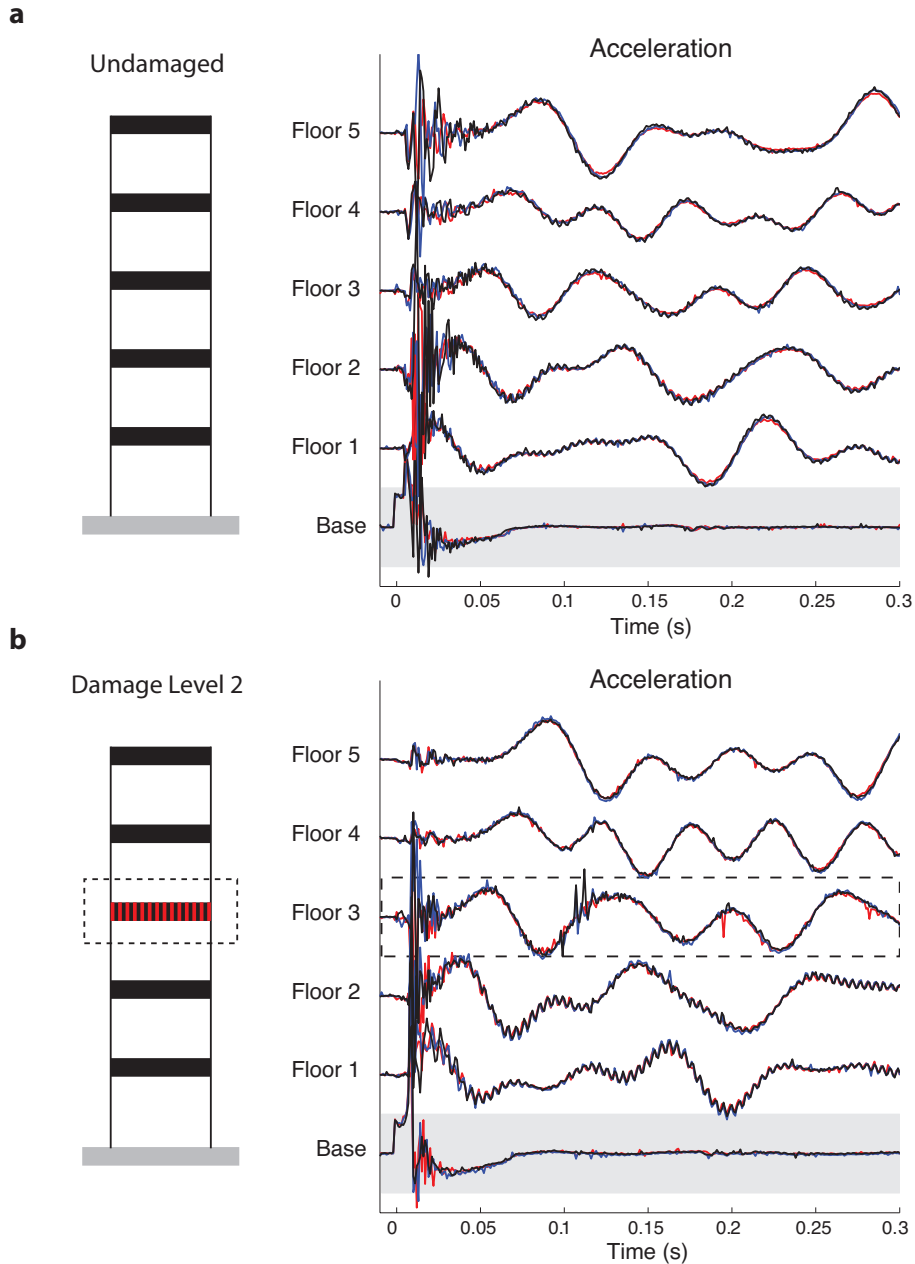


Figure 3.3: **Consistency Between Trials.** **a.** The undamaged shear beam is subjected to a pulse at its base via a shake table. Three separate trials are compared in each plot, and considerable agreement is shown between trials. **b.** The damaged (Damage Level 2 at Floor 3) shear beam is subjected to a pulse at its base via a shake table. Again, there is considerable agreement shown between trials. There are minor differences in the occurrence of the transient signals, such as those present in the third floor accelerations at times 0.12 seconds and 0.2 seconds. These transient signals are presumably caused by mechanical slippage and impact at the loosened connections, and the signals are clearly observed over the modal response of the structure. There is also a less efficient transmission of high-frequency motion through the third floor, as can be seen by the amplitudes of the high-frequency acceleration that accompany the initial pulse generated by the shake table at time 0.015 seconds; the high-frequency energy seems to become trapped within the first and second floors. The relative amplitudes in each plot have been preserved, as the acceleration time series have been scaled proportional to the maximum amplitude of the initial pulse at the ground floor.

the displacement vector  $x(t)$  and the force vector  $f(t)$  are given by:

$$\begin{aligned} x(t) &= \begin{pmatrix} x_1(t) & x_2(t) & x_3(t) & x_4(t) & x_5(t) \end{pmatrix}^T, \\ f(t) &= \begin{pmatrix} f_1(t) & f_2(t) & f_3(t) & f_4(t) & f_5(t) \end{pmatrix}^T. \end{aligned}$$

A schematic of both the undamaged and damaged shear beam models is shown in Figure 3.2.

### 3.2.1 Undamaged Frame

Assuming moment connections and uniform properties, the mass and stiffness matrices for the undamaged frame are populated.

$$\begin{aligned} M &= m \begin{pmatrix} 1 & 0 & 0 & 0 & 0 \\ 0 & 1 & 0 & 0 & 0 \\ 0 & 0 & 1 & 0 & 0 \\ 0 & 0 & 0 & 1 & 0 \\ 0 & 0 & 0 & 0 & 1 \end{pmatrix}, \\ K &= k \begin{pmatrix} 2 & -1 & 0 & 0 & 0 \\ -1 & 2 & -1 & 0 & 0 \\ 0 & -1 & 2 & -1 & 0 \\ 0 & 0 & -1 & 2 & -1 \\ 0 & 0 & 0 & -1 & 1 \end{pmatrix}. \end{aligned}$$

The model parameters used for the floor mass  $m$  and interstory shear stiffness  $k$  are determined both theoretically, by using the properties of aluminum and the dimensions of the experimental model, and experimentally. The experimental value for the mass  $m$  is obtained by disconnecting and weighing one of the floors of the structure and is measured to be 0.9355 kg. The corresponding theoretical value is found by multiplying the volume of a

floor by the density of aluminum (2.7 g/cm<sup>3</sup>) and is calculated to be 1.008 kg. The weight of the columns is neglected. The stiffness value  $k$  is determined theoretically by approximating the column as an Euler-Bernoulli beam, using the material properties of aluminum and the geometry of the experimental model, and is calculated to be  $2.993 \cdot 10^3$  N/m.

Let  $\lambda_n$  and  $\phi_n$ , for  $n = 1, 2, 3, 4, 5$ , denote the distinct eigenvalues and eigenvectors (normalized with respect to the mass matrix) of  $M^{-1}K$ .

$$\begin{aligned} \Phi &= \begin{pmatrix} \phi_1 & \phi_2 & \phi_3 & \phi_4 & \phi_5 \end{pmatrix}, \\ \lambda_n &= \omega_n^2 \\ &= (2\pi f_n)^2, \\ M_g &= \Phi^T M \Phi \\ &= I_{5 \times 5}, \\ K_g &= \Phi^T K \Phi \\ &= \begin{pmatrix} \omega_1^2 & 0 & 0 & 0 & 0 \\ 0 & \omega_2^2 & 0 & 0 & 0 \\ 0 & 0 & \omega_3^2 & 0 & 0 \\ 0 & 0 & 0 & \omega_4^2 & 0 \\ 0 & 0 & 0 & 0 & \omega_5^2 \end{pmatrix}. \end{aligned}$$

The generalized coordinate vector  $x(t)$  is expressed in terms of the principal coordinate displacement vector  $p(t)$ . By converting from generalized coordinates  $x$  to principal coordinates  $p$ , the differential equations of motions can be uncoupled.

$$\begin{aligned} x(t) &= \Phi p(t), \\ p(t) &= \Phi^{-1} x(t), \\ p(t) &= I p(t) \\ &= \Phi^T M \Phi p(t) \\ &= \Phi^T M x(t). \end{aligned}$$

Assume modal damping, with a modal damping value for the  $n^{th}$  mode shape denoted by  $\zeta_n$ . The damping matrix  $C$  and the damped natural frequencies  $\omega^d$  are given by:

$$\begin{aligned}
C_{modal} &= \begin{pmatrix} 2\zeta_1\omega_1 & 0 & 0 & 0 & 0 \\ 0 & 2\zeta_2\omega_2 & 0 & 0 & 0 \\ 0 & 0 & 2\zeta_3\omega_3 & 0 & 0 \\ 0 & 0 & 0 & 2\zeta_4\omega_4 & 0 \\ 0 & 0 & 0 & 0 & 2\zeta_5\omega_5 \end{pmatrix} & (3.2) \\
&= \Phi^T C \Phi, \\
C_{modal} &= I C_{modal} I \\
&= \Phi^T M \Phi C_{modal} \Phi^T M \Phi \\
&= \Phi^T (M \Phi C_{modal} \Phi^T M) \Phi, \\
C &= M \Phi C_{modal} \Phi^T M \\
&= \Phi^{-T} C_{modal} \Phi^{-1}, \\
\omega_n^d &= \omega_n \sqrt{1 - \zeta_n^2}.
\end{aligned}$$

Modal damping is assumed for the numerical model, and the values are also determined experimentally by integrating to obtain the displacement, applying the logarithmic decrement method to estimate modal damping for the first mode and the half-power bandwidth method to estimate modal damping for higher modes (Cole, 1971). The theoretical values for damping are calculated assuming 2% proportional modal damping.

The differential equations of motion, Equation 3.1, are uncoupled by transforming to principal coordinates and multiplying the equation by  $\Phi^T$ :

$$\begin{aligned}
\Phi^T M \Phi \ddot{p}(t) + \Phi^T C \Phi \dot{p}(t) + \Phi^T K \Phi p(t) &= \Phi^T f(t), \\
M_g \ddot{p}(t) + C_{modal} \dot{p}(t) + K_g p(t) &= \Phi^T f(t).
\end{aligned}$$

Letting  $g_n(t)$  denote the  $n^{th}$  generalized force term (the  $n^{th}$  component of the vector

$\Phi^T f(t)$ ), each of the five uncoupled equations is written as:

$$\ddot{p}_n(t) + 2\zeta_n\omega_n\dot{p}_n(t) + \omega_n^2 p_n(t) = g_n(t). \quad (3.3)$$

### 3.2.2 Damaged Frame

Damage is introduced at a given floor by loosening the screws connecting the columns to the floor. Damage is only introduced to one floor at a time; the other four floors and base remain undamaged. In Damage Levels 1, 2, and 3, all six screws connecting the columns to a floor are loosened, by 1/6, 2/6, and 3/6 turn, respectively. The amount of space created by loosening the screws is very small. By loosening the screws to create damage, a short gap of length 0.21 mm (0.008”), 0.42 mm (0.017”), and 0.64 mm (0.025”) is created on either side of the damaged floor for Damage Levels 1, 2, and 3, respectively.

Damage to the system is modeled either as damage to the connection or as damage to the columns: I) in Damage Model I, the original moment connection at the damaged floor is replaced by a semi-rigid connection, and II) in Damage Model II, a reduction in inter-story shear stiffness is introduced in the columns directly above and below the damaged floor. Schematics of the damage models are shown in Figure 3.2.

The damage models are used to estimate the amount of damage from a static tilt test and from a dynamic impulse test, and give insight into the mechanism of damage, as an exact physical explanation for quantifying the amount of damage is unavailable. The percent change in inter-story stiffness in an actual building due to structural damage could range from a small percentage, in the case of damage to a few structural members at a floor, to a large percentage, in the case of severe damage to a floor. It is important to quantify the loss of stiffness that is present in the damaged shear beam in order to evaluate whether the amount of damage is analogous to realistic losses of inter-story shear stiffness that could be encountered in an actual civil structure, due to failure of structural members on that story during an earthquake, or due to the progression of damage in a structure due to environmental loading.

### 3.2.2.1 Damage Model I

In Damage Model I, a reduction in stiffness is introduced at the beam-column connections at the damaged floor by replacing the moment connections with semi-rigid connections. The system still obeys the differential equations of motions given by Equation 3.1, but the changes in boundary conditions at each floor are manifested in the stiffness matrix. The stiffness matrix is updated according to the new lateral stiffness calculated while taking the new boundary conditions into account. The mass matrix remains the same, but damping is expected to increase, and is determined experimentally. In the matrices below,  $K_m^I$  represents the stiffness matrix for the structure with damage to the  $m^{th}$  floor and assuming Damage Model I. The level of damage is parameterized by introducing the scalar  $\kappa$  to represent a torsion spring at the damaged connection, thus representing a semi-rigid connection. The values for stiffness are calculated by approximating the column as a Euler-Bernoulli beam, introducing a torsion spring at the damaged connection, and assuming a small angle of rotation at the connection.

$$K_1^I = k \begin{pmatrix} 2 & -1 & 0 & 0 & 0 \\ -1 & \frac{13+2\kappa}{8+\kappa} & -1 & 0 & 0 \\ 0 & -1 & 2 & -1 & 0 \\ 0 & 0 & -1 & 2 & -1 \\ 0 & 0 & 0 & -1 & 1 \end{pmatrix}, K_2^I = k \begin{pmatrix} \frac{13+2\kappa}{8+\kappa} & -1 & \frac{3}{8+\kappa} & 0 & 0 \\ -1 & 2 & -1 & 0 & 0 \\ \frac{3}{8+\kappa} & -1 & \frac{13+2\kappa}{8+\kappa} & -1 & 0 \\ 0 & 0 & -1 & 2 & -1 \\ 0 & 0 & 0 & -1 & 1 \end{pmatrix},$$

$$K_3^I = k \begin{pmatrix} 2 & -1 & 0 & 0 & 0 \\ -1 & \frac{13+2\kappa}{8+\kappa} & -1 & \frac{3}{8+\kappa} & 0 \\ 0 & -1 & 2 & -1 & 0 \\ 0 & \frac{3}{8+\kappa} & -1 & \frac{13+2\kappa}{8+\kappa} & -1 \\ 0 & 0 & 0 & -1 & 1 \end{pmatrix}, K_4^I = k \begin{pmatrix} 2 & -1 & 0 & 0 & 0 \\ -1 & 2 & -1 & 0 & 0 \\ 0 & -1 & \frac{13+2\kappa}{8+\kappa} & -1 & \frac{3}{8+\kappa} \\ 0 & 0 & -1 & 2 & -1 \\ 0 & 0 & \frac{3}{8+\kappa} & -1 & \frac{5+\kappa}{8+\kappa} \end{pmatrix},$$

$$K_5^I = k \begin{pmatrix} 2 & -1 & 0 & 0 & 0 \\ -1 & 2 & -1 & 0 & 0 \\ 0 & -1 & 2 & -1 & 0 \\ 0 & 0 & -1 & \frac{5+2\kappa}{4+\kappa} & -\frac{1+\kappa}{4+\kappa} \\ 0 & 0 & 0 & -\frac{1+\kappa}{4+\kappa} & \frac{1+\kappa}{4+\kappa} \end{pmatrix}.$$

To work with a more manageable stiffness parameter that ranges from 0 to 1, introduce stiffness parameter  $\gamma$ :

$$\kappa = \frac{\gamma}{1-\gamma}. \quad (3.4)$$

As  $\gamma$  ranges from 0 to 1, the connection changes from a simple connection (no torsional stiffness, i.e.,  $\kappa = 0$ ) to a moment connection (infinite torsional stiffness, i.e.,  $\kappa \rightarrow \infty$ ). For a moment connection, the stiffness matrices simplify to those for the undamaged case. For a simple connection, the stiffness matrices simplify to those shown below:

$$K_1^I|_{\kappa=0} = k \begin{pmatrix} 2 & -1 & 0 & 0 & 0 \\ -1 & 13/8 & -1 & 0 & 0 \\ 0 & -1 & 2 & -1 & 0 \\ 0 & 0 & -1 & 2 & -1 \\ 0 & 0 & 0 & -1 & 1 \end{pmatrix}, K_2^I|_{\kappa=0} = k \begin{pmatrix} 13/8 & -1 & 3/8 & 0 & 0 \\ -1 & 2 & -1 & 0 & 0 \\ 3/8 & -1 & 13/8 & -1 & 0 \\ 0 & 0 & -1 & 2 & -1 \\ 0 & 0 & 0 & -1 & 1 \end{pmatrix},$$

$$K_3^I|_{\kappa=0} = k \begin{pmatrix} 2 & -1 & 0 & 0 & 0 \\ -1 & 13/8 & -1 & 3/8 & 0 \\ 0 & -1 & 2 & -1 & 0 \\ 0 & 3/8 & -1 & 13/8 & -1 \\ 0 & 0 & 0 & -1 & 1 \end{pmatrix}, K_4^I|_{\kappa=0} = k \begin{pmatrix} 2 & -1 & 0 & 0 & 0 \\ -1 & 2 & -1 & 0 & 0 \\ 0 & -1 & 13/8 & -1 & 3/8 \\ 0 & 0 & -1 & 2 & -1 \\ 0 & 0 & 3/8 & -1 & 5/8 \end{pmatrix},$$

$$K_5^I|_{\kappa=0} = k \begin{pmatrix} 2 & -1 & 0 & 0 & 0 \\ -1 & 2 & -1 & 0 & 0 \\ 0 & -1 & 2 & -1 & 0 \\ 0 & 0 & -1 & 5/4 & -1/4 \\ 0 & 0 & 0 & -1/4 & 1/4 \end{pmatrix}.$$

### 3.2.2.2 Damage Model II

In Damage Model II, a reduction in inter-story shear stiffness is introduced in the columns directly above and below the damaged floor. Unlike Damage Model I, the moment connection is assumed to be undamaged, but the columns immediately above and below are assumed to have the same reduced lateral stiffness, with a value that is denoted by  $k_d$ . The stiffness parameter for this model is chosen to be the ratio  $k_d/k$ , and it also ranges from 0 (no stiffness) to 1 (no loss in stiffness).

$$K_1^{II} = k \begin{pmatrix} 2k_d/k & -k_d/k & 0 & 0 & 0 \\ -k_d/k & k_d/k + 1 & -1 & 0 & 0 \\ 0 & -1 & 2 & -1 & 0 \\ 0 & 0 & -1 & 2 & -1 \\ 0 & 0 & 0 & -1 & 1 \end{pmatrix}, K_2^{II} = k \begin{pmatrix} 1 + k_d/k & -k_d/k & 0 & 0 & 0 \\ -k_d/k & 2k_d/k & -k_d/k & 0 & 0 \\ 0 & -k_d/k & 1 + k_d/k & -1 & 0 \\ 0 & 0 & -1 & 2 & -1 \\ 0 & 0 & 0 & -1 & 1 \end{pmatrix},$$

$$K_3^{II} = k \begin{pmatrix} 2 & -1 & 0 & 0 & 0 \\ -1 & 1 + k_d/k & -k_d/k & 0 & 0 \\ 0 & -k_d/k & 2k_d/k & -k_d/k & 0 \\ 0 & 0 & -k_d/k & 1 + k_d/k & -1 \\ 0 & 0 & 0 & -1 & 1 \end{pmatrix},$$

$$K_4^{II} = k \begin{pmatrix} 2 & -1 & 0 & 0 & 0 \\ -1 & 2 & -1 & 0 & 0 \\ 0 & - & 1 + k_d/k & -k_d/k & 0 \\ 0 & 0 & -k_d/k & 2k_d/k & -k_d/k \\ 0 & 0 & 0 & -k_d/k & k_d/k \end{pmatrix}, K_5^{II} = k \begin{pmatrix} 2 & -1 & 0 & 0 & 0 \\ -1 & 2 & -1 & 0 & 0 \\ 0 & -1 & 2 & -1 & 0 \\ 0 & 0 & -1 & 1 + k_d/k & -k_d/k \\ 0 & 0 & 0 & -k_d/k & k_d/k \end{pmatrix}.$$

In Section 3.3.2, these models are used to estimate the reduction in stiffness that is caused by damage.

### 3.3 Experimental Results

The following experimental results are presented.

**Section 3.3.1** A set of experiments is conducted to verify the linearity of the damaged and undamaged frame.

**Section 3.3.2** A series of static tilt tests is performed. The stiffness of the damaged and undamaged frames is estimated, and the amount of damage at each damage level (expressed as a ratio of stiffnesses) is computed as a ratio of stiffnesses.

**Section 3.3.3** A series of dynamic testing is performed with the frame damaged at each floor at Damage Levels 1-3. Experimental results are shown for the undamaged frame, and the damaged frame, at three different levels of damage. The raw and filtered acceleration records are used for the time series analysis. Four repeated trials are conducted for each damage case. The set of experiments was conducted with sampling rates of 1 ksps, 5 ksps, and 150 ksps.

**Section 3.3.4** A damage detection method is discussed, and a series of dynamic tests are conducted in which damage is sequentially introduced to the frame, one bolt at a time. A damage-detection method is presented and used to identify potential damage in the frame.

**Section 3.3.5** A comparison of the experimental and theoretical data is presented, for the frequency domain (i.e., mode shapes and modal frequencies) for the undamaged frame.

### 3.3.1 Linearity of the Damaged and Undamaged Shear Beam

Before applying techniques developed for a linear system, it is necessary to first verify that the shear beam behaves as a linear system. A linear system is one in which the doubling of the magnitude of the excitation force results in a doubling of the response, and the response to two simultaneous inputs equals the sum of the responses to each independent input.

One way to test linearity is by inputting a pure sinusoidal signal at the base of the shear beam. If the structure behaves linearly, then the response of the structure will consist of a signal of only the input frequency. If the structure behaves nonlinearly, then either harmonic distortion or frequency modulation will occur, and harmonics or sidebands will be present in the frequency response of the structure (Farrar et al., 2007). As the shake table used is not capable of inputting a pure sinusoidal wave, a different approach must be taken. According to Ewins (1984), signs of nonlinear behavior include the following: 1) natural frequencies vary with position and strength of excitation, 2) distorted frequency response plots, and 3) unstable or unrepeatably data. The structure is thus subjected to a pulse at its base, and the natural frequencies and modeshapes are analyzed for changes.

As seen in Figure 3.4, across a range in shake table gains from 2 to 6, there is no variation in the observed natural frequencies and little variation in the observed modeshapes for the undamaged shear beam. For the damaged shear beam (Damage Level 1 introduced at the third floor), there is a slight decrease in the observed natural frequencies above a shake table gain of 4. In order to remain within the linear response range of the shear beam, while maintaining a high signal-to-noise ratio (which increases with an increased shake table gain), a shake table gain of either 3 or 4 is used for the experiments in this chapter. There is a possibility that the shaking of the structure causes the bolts to slightly loosen, however only small variations in observed natural frequencies are observed between repeated trials.

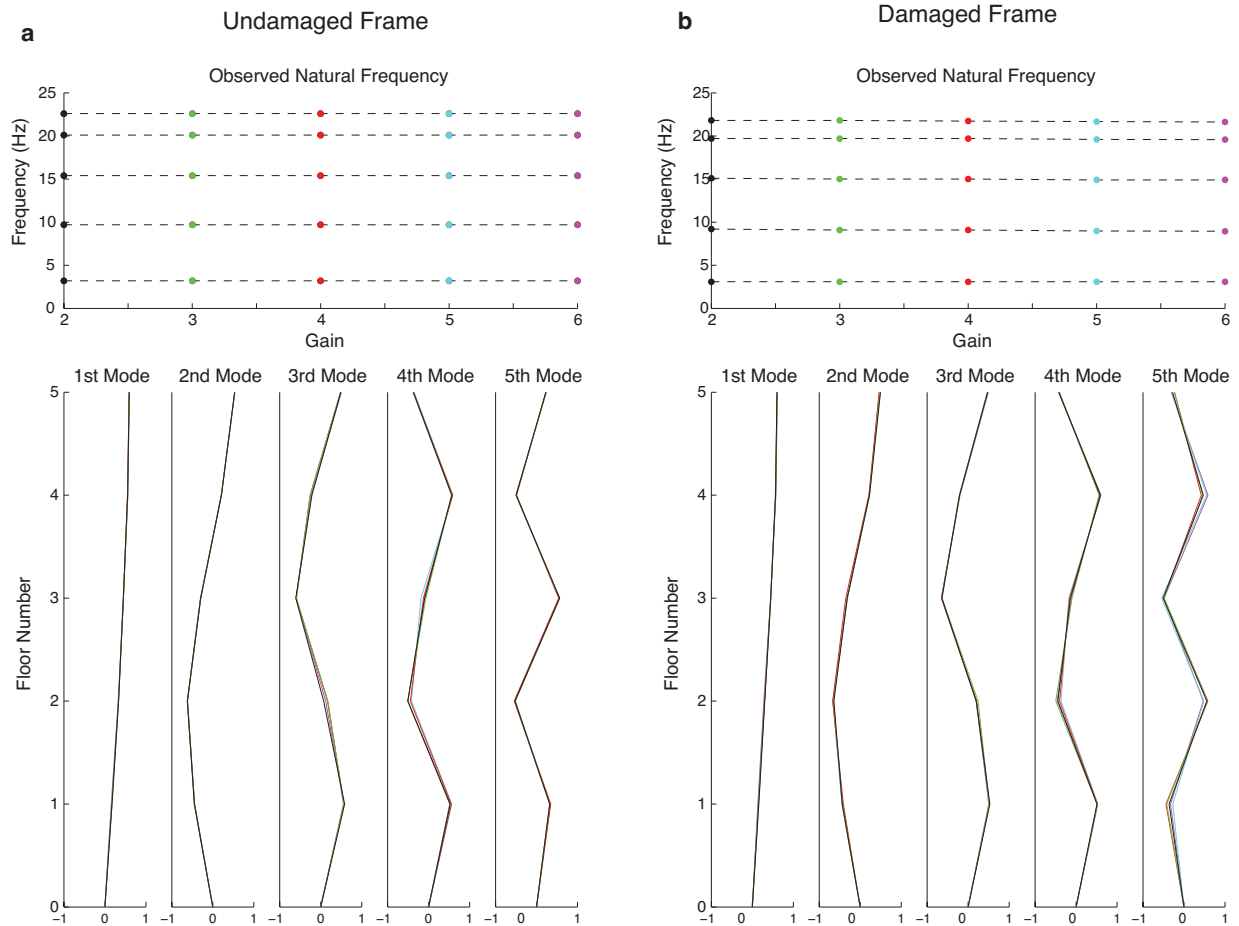


Figure 3.4: **Verification of System Linearity.** **a.** The undamaged shear beam is subjected to a series of pulses at its base, over a range of shake table gains, and the modal properties are compared. There is no change in the observed natural frequencies over the frequency range of interest, and the mass-normalized modeshapes are also consistent. **b.** Damage (Damage Level I) is introduced at the third floor, and the damaged shear beam is subjected to a similar series of pulses. The frequencies are unchanged until a gain of 4, after which there is a slight decrease in two of the natural frequencies. The modeshapes are consistent between rounds.

### 3.3.2 Static Testing:

#### Stiffness Parameter Estimation via a Tilt Test

The stiffness and stiffness parameters are determined experimentally by performing a tilt test. Complementing the dynamic testing of the structure, the tilt test provides an additional method to estimate the stiffness for the small-scale structure by using its static response. The undamaged model is rotated from  $-30^\circ$  to  $30^\circ$  using a tilt table that rotates the structure at precise angles, shown in Figure 3.5. The lateral force on each floor due to gravity can be calculated using the measured mass of each floor. The structure is in static equilibrium; its velocity and acceleration equals zero, and the resulting displacement at the top floor,  $x_{5\text{ tilt}}$ , is recorded. The differential equation of motion, Equation 3.1, for the static case is:

$$Kx = f. \quad (3.5)$$

Solving for  $x$  by multiplying the equation by  $K^{-1}$  and substituting in the experimentally-measured value  $m_{exp}$  for  $m$  yields:

$$\begin{aligned} x_{\text{tilt}}(\theta) &= \frac{mg \sin \theta}{k} \begin{pmatrix} 2 & -1 & 0 & 0 & 0 \\ -1 & 2 & -1 & 0 & 0 \\ 0 & -1 & 2 & -1 & 0 \\ 0 & 0 & -1 & 2 & -1 \\ 0 & 0 & 0 & -1 & 1 \end{pmatrix}^{-1} \begin{pmatrix} 1 \\ 1 \\ 1 \\ 1 \\ 1 \end{pmatrix} \\ &= \frac{mg \sin \theta}{k} \begin{pmatrix} 1 & 1 & 1 & 1 & 1 \\ 1 & 2 & 2 & 2 & 2 \\ 1 & 2 & 3 & 3 & 3 \\ 1 & 2 & 3 & 4 & 4 \\ 1 & 2 & 3 & 4 & 5 \end{pmatrix} \begin{pmatrix} 1 \\ 1 \\ 1 \\ 1 \\ 1 \end{pmatrix} \\ &= \frac{mg \sin \theta}{k} (5 \ 9 \ 12 \ 14 \ 15)^T, \\ k &= \frac{15mg \sin \theta}{x_{5\text{ tilt}}}. \end{aligned} \quad (3.6)$$

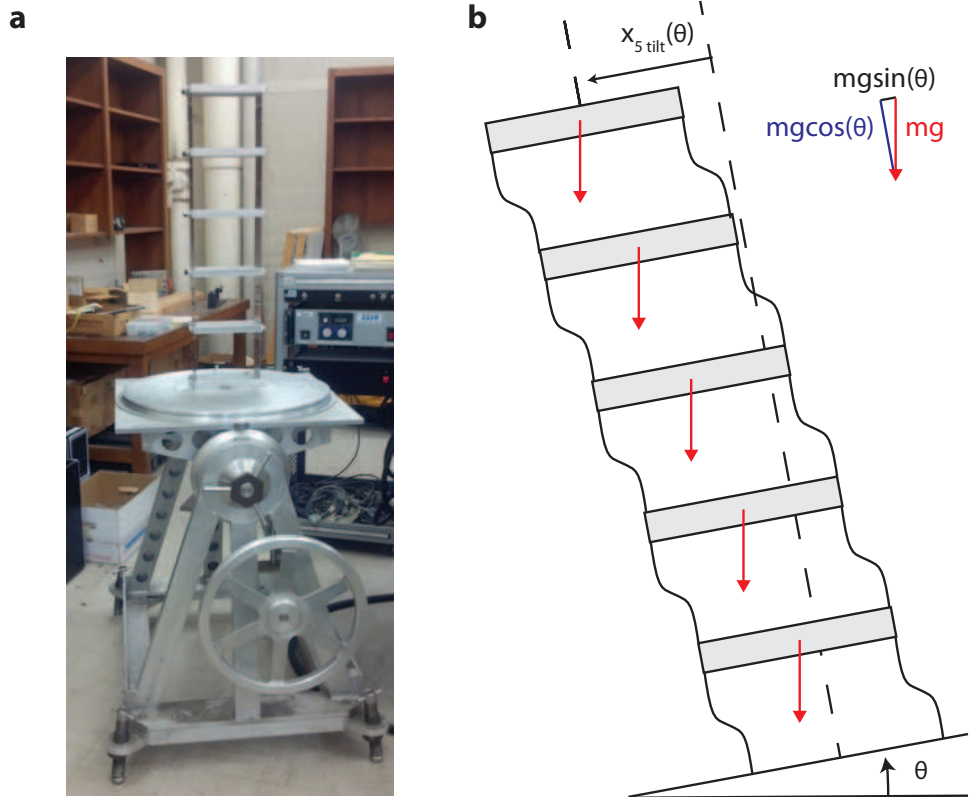


Figure 3.5: **Static Testing: Tilt Table and Schematic** **a**, The test structure is firmly fixed at its base to a tilt table that precise controls the angle of tilt. The resulting relative displacement at the top of the structure is determined for various angles between  $-30^\circ$  and  $30^\circ$ . **b** The lateral force is determined from the tilt angle and weight of the structure

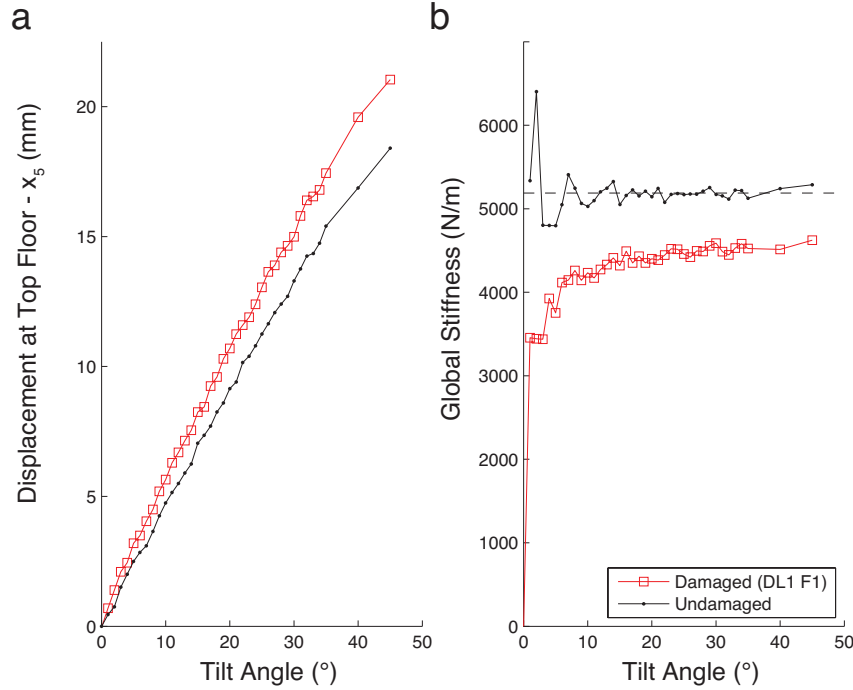


Figure 3.6: **Tilt Test: Damaged vs. Undamaged (Example)**. The resulting roof displacement for the undamaged and damaged (Damage Level 1 introduced at Floor 1) frame is shown to the left. To the right, the global stiffness, calculated using Equation 3.6, is plotted for each point. As expected, the damaged structure experiences larger displacements and hence has reduced global stiffness than the undamaged structure. The mean value of the global stiffness,  $k_{exp} = 5.19 \times 10^3 \text{ N/m}$ , for the undamaged case is indicated by the dashed line.

When performing a matrix inversion, it is important to check the condition number. The condition number is used to estimate the accuracy of the results of the inversion and, for a matrix, is equal to the ratio of the largest singular value to the smallest singular value. The condition number for  $K$  is calculated to be 45, or  $10^{3.8}$ , which is a reasonably small value. This means that about four digits of accuracy might be lost in addition to the loss of precision from arithmetic methods; the larger the condition number, the more ill-conditioned the system (Cheney and Kincaid, 2012).

A set of tilt tests is performed for each of the 15 damaged configurations of the structure in order to assess the change in stiffness and corresponding value of the stiffness parameter that accompanies the level and location of damage. The displacement at the top floor,  $x_{5 \text{ tilt}}$ , is recorded when the damaged shear beam is rotated through various angles between  $-30^\circ$

and 30°. The stiffness at the undamaged floors is assumed to be equal to the experimentally-obtained undamaged stiffness  $k_{exp}$ . For each data point, the stiffness parameter is solved for using Equation 3.5, and the stiffness parameter depends on which model of damage is used. For Damage Model I, the stiffness parameter estimated is  $\gamma$ , given by Equation 3.4; for Damage Model II, the stiffness parameter estimated is the ratio of the reduced stiffness value to the undamaged stiffness value  $k_d/k$ .

As inverting the stiffness matrices for the damaged frame is more difficult than it was for the undamaged case, the inversion is formulated as a numerical optimization problem. For damage introduced at the  $n^{th}$  floor, using stiffness matrix  $K$  for the undamaged system with stiffness value  $k_{exp}$ , and assuming Damage Model I, the stiffness parameter  $\gamma$  is estimated as:

$$\gamma_{tilt} = \arg \min_{\gamma \in [0,1]} |x_{5\ tilt} - \begin{pmatrix} 0 & 0 & 0 & 0 & 1 \end{pmatrix} K_{damaged}^{-1}(k_{exp}, \gamma) f_g|^2.$$

The term ‘arg min’ simply means the value of  $\gamma$  within the range of [0 1] that minimizes the argument to the right of the expression. Stiffness matrix  $K_{damaged}$  is written as  $K_{damaged}^{-1}(k_{exp}, \gamma)$  to emphasize its dependence on the parameters. The force vector  $f_g$  is a 5x1 vector of forces due to gravity, with each term equal to  $m_{exp}g$ .

Similarly, assuming Damage Model II under the same conditions, the stiffness parameter  $k_d/k$  is estimated as:

$$(k_d/k)_{tilt} = \frac{1}{k_{exp}} \arg \min_{k_d \in [0, k_{exp}]} |x_{5\ tilt} - \begin{pmatrix} 0 & 0 & 0 & 0 & 1 \end{pmatrix} K_{2,n}^{-1}(k_{exp}, k_d) f_g|^2.$$

The estimated values for the stiffness parameters, listed in Table 3.2 and plotted in Figure 3.7, can be used as reference values in relating differences observed in the dynamic response of the structure to the reduction in stiffness of the frame. Moderate levels of damage are created by the slight loosening of the bolts. If damage is modeled as a loss of stiffness in the connection, as in Damage Model I, then as expected, higher values of  $\gamma$  are observed for lower levels of damage. This means that the damaged connection behaves more like a simple

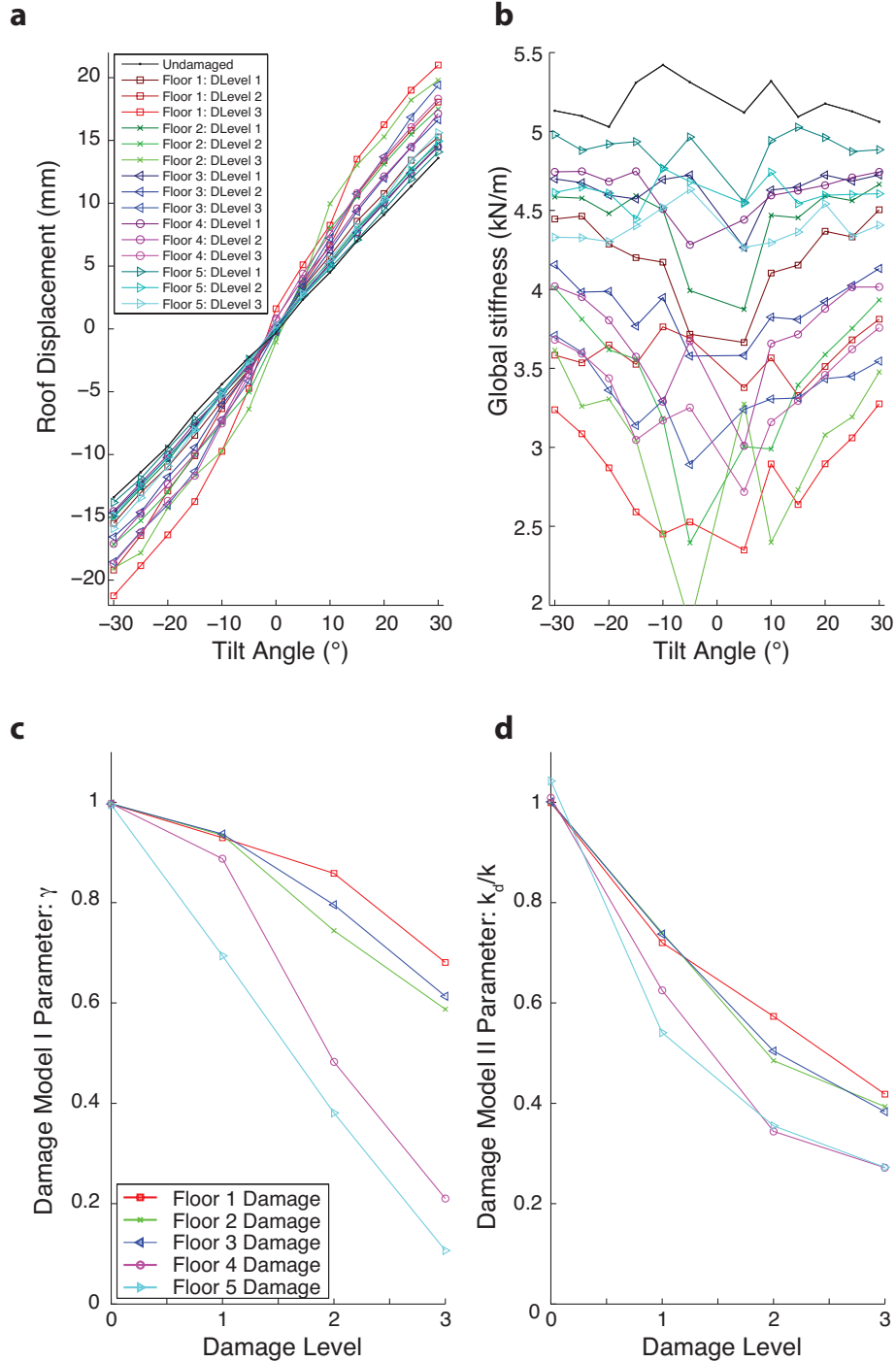


Figure 3.7: **Tilt Test: Damaged vs. Undamaged (All Cases)**. **a**, The undamaged or damaged (Levels 1-3, Floors 1-5) structure is tilted at various angles between  $-30^\circ$  and  $30^\circ$ , and the resulting roof displacement is recorded. **b**, The global stiffness is determined using Equation 3.6. As expected, the undamaged model has the highest global stiffness, with the global stiffness decreasing from Levels 1 to 2 and 3. **c** Damage Model I is assumed, and the tilt angle and recorded displacement are used to solve for the stiffness parameter, as in Equation 3.7. **d** Damage Model II is assumed, and the tilt angle and recorded displacement are used to solve for the stiffness parameter, as in Equation 3.7. As expected, the stiffness parameter decreases with increasing damage. The stiffness parameters for damage introduced to Floors 4 and 5 are lower than those estimated for damage to Floors 1, 2, and 3.

connection and less like a moment connection for higher levels of damage than it does for lower levels of damage. If instead damage is modeled as a loss of interstory stiffness adjacent to the damaged floor, then higher values of  $k_d/k$  are observed for lower levels of damage. This means that, for lower levels of damage, the stiffness of the damaged columns is closer to that of the undamaged columns, and the column stiffness decreases for higher levels of damage.

| Level of<br>Damage | Model Type<br>and Parameter | Damaged Floor |      |      |      |      |
|--------------------|-----------------------------|---------------|------|------|------|------|
|                    |                             | 1             | 2    | 3    | 4    | 5    |
| Undamaged          | DM I: $\gamma$              | 1.00          | 1.00 | 1.00 | 1.00 | 1.00 |
|                    | DM II: $k_d/k$              | 1.00          | 1.00 | 1.00 | 1.01 | 1.04 |
| Level 1            | DM I: $\gamma$              | 0.93          | 0.93 | 0.94 | 0.89 | 0.69 |
|                    | DM II: $k_d/k$              | 0.72          | 0.74 | 0.74 | 0.63 | 0.54 |
| Level 2            | DM I: $\gamma$              | 0.86          | 0.74 | 0.80 | 0.48 | 0.38 |
|                    | DM II: $k_d/k$              | 0.57          | 0.49 | 0.50 | 0.34 | 0.36 |
| Level 3            | DM I: $\gamma$              | 0.68          | 0.59 | 0.61 | 0.21 | 0.11 |
|                    | DM II: $k_d/k$              | 0.42          | 0.39 | 0.38 | 0.27 | 0.27 |

Table 3.1: **Estimated Stiffness Parameters from the Tilt Test.** To quantify the amount of damage introduced to the frame in Damage Levels 1-3, a static tilt test is performed, and a model for damage is assumed. The tilt angle and resulting rotation is used with the model to determine the amount of stiffness in the damaged connection. Moderate levels of damage are created by the slight loosening of the bolts.

In addition to the expected trend of decreasing stiffness with increasing levels of damage, there appears to be a trend of decreasing stiffness for damage to increasing floor numbers for a given level of damage. We expect stiffness values to be uniform across different floors for the same level of damage. The general trends in the table suggest that there is a phenomenon that exists in the real system, such as rotation or a nonlinear stiffness mechanism, that is not captured by the simple damage models.

Finally, if damage is introduced by the loosening of only one screw, then the amount of

displacement at the top floor for a given angle of rotation is observed to equal the amount of displacement at the top floor for the undamaged frame. This means that there is no observed loss of inter-story stiffness for this damage case.

### 3.3.3 Dynamic Testing: Damage Levels 1, 2, and 3

The shear beam is excited by a repeatable pulse at its base by a shake table. By using a repeatable pulse at the base, the baseline response of the frame in an undamaged configuration can be directly compared to the response of the frame for levels of increasing damage. Differences in the dynamic response of the structure between trials due to differences in the source are minimized, and the effect of damage on the dynamic response of the structure can be more readily analyzed.

As mentioned previously, in Damage Levels 1, 2, and 3, damage is introduced to the shear beam by incrementally loosening the six screws attaching the two columns to one of the five floors. Damage Levels 1, 2, and 3 correspond to a 1/6, 2/6, and 3/6 turn of each screw at the damaged floor, respectively. The amount of space created by loosening the screws is very small. The length of the gap created on one side is equal to 0.21 mm (0.0083"), 0.42 mm (0.017"), and 0.64 mm (0.025") for Damage Levels 1, 2, and 3, respectively.

A schematic of the typical dynamic response recorded at 1 ksps is shown in Figure 3.8. The pulse at the base of the structure excites a shear wave that travels up the height of the building and is reflected at the top. The response of the structure can be filtered into its low-frequency and high-frequency components. The low-frequency component consists of the predominant modal response of the structure that includes the five lowest modes. The high-frequency component consists of the initial slip of the shake table as well as mechanical slippage and impact that occurs at the damaged floor. When the screws are loosened, the gap allows for motion of the columns and washers.

The unfiltered dynamic response of the frame in all 15 damaged cases (three levels of damage, five different damage locations) is plotted against the undamaged case in Figure 3.9. A few features in the damaged data stand out. The low-frequency response of the

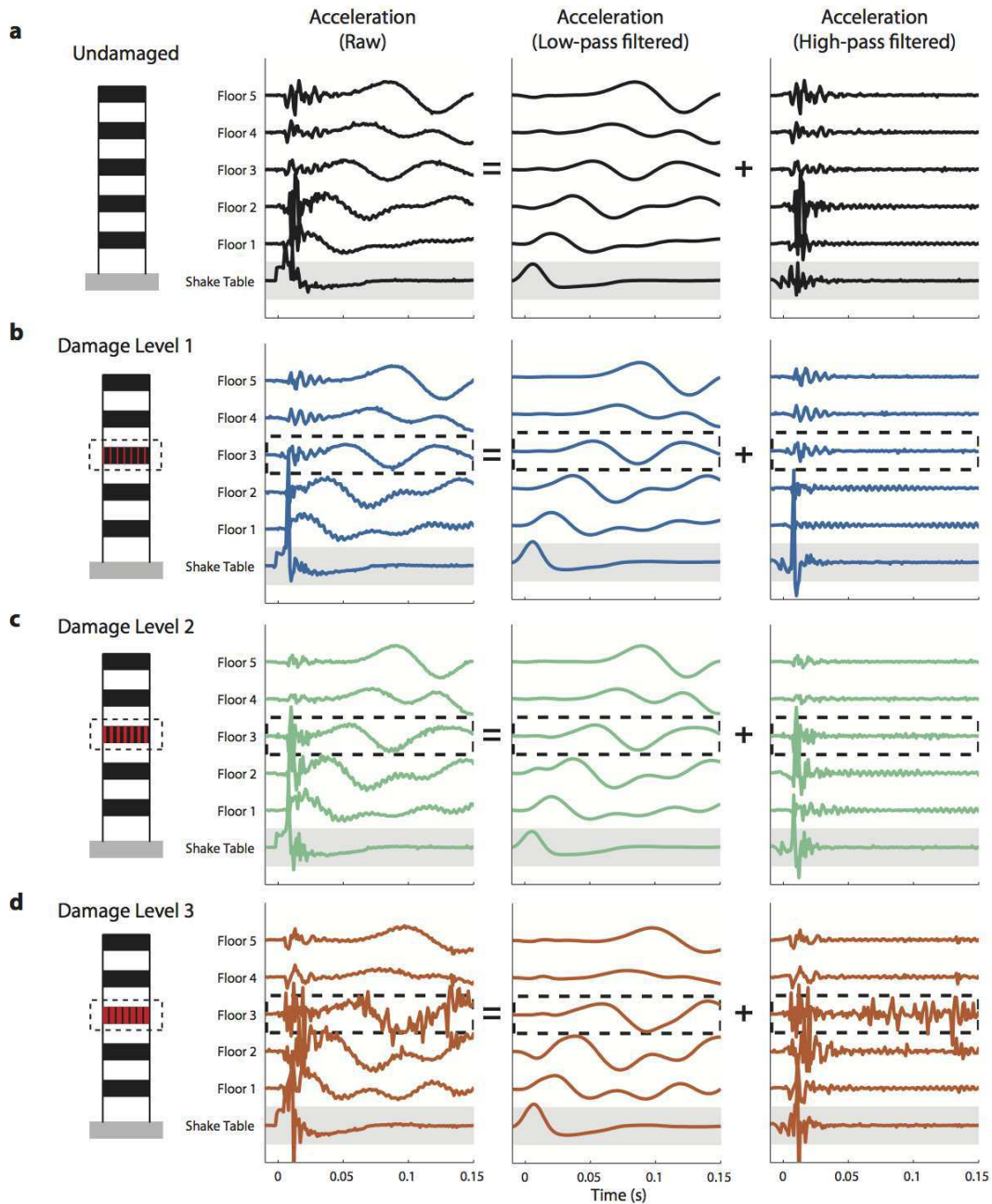


Figure 3.8: **Dynamic Testing: Explanatory Schematic.** The shear beam is excited by a repeatable pulse at its base by a shake table. Three different levels of damage are introduced into one floor of the the shear beam; in this case Floor 3 is damaged. A total of six accelerometers instrument the shear beam, one attached to each floor and one attached to the shake table; the sampling rate is 1 kps. By using a repeatable pulse at the base, the response of the frame in an **a** undamaged configuration can be directly compared to the response of the frame for levels of increasing damage (**b** Damage Level 1, **c** Damage Level 2, **d** Damage Level 3). The response of the structure is filtered into its low-frequency and high-frequency components. The low-frequency response of the structure consists of the predominant modal response (first five modes) and is obtained using a 4<sup>th</sup> order Butterworth filter with a 50 Hz cutoff frequency. The high-frequency response is obtained by applying a 4<sup>th</sup> order high-pass Butterworth filter. The high-frequency components decay much more rapidly than do the low-frequency components. The primary sources of the high-frequency signals are the initial slip of shake table as well as mechanical slippage and impact at the damaged floor. These data were recorded at a rate of 5 kps.

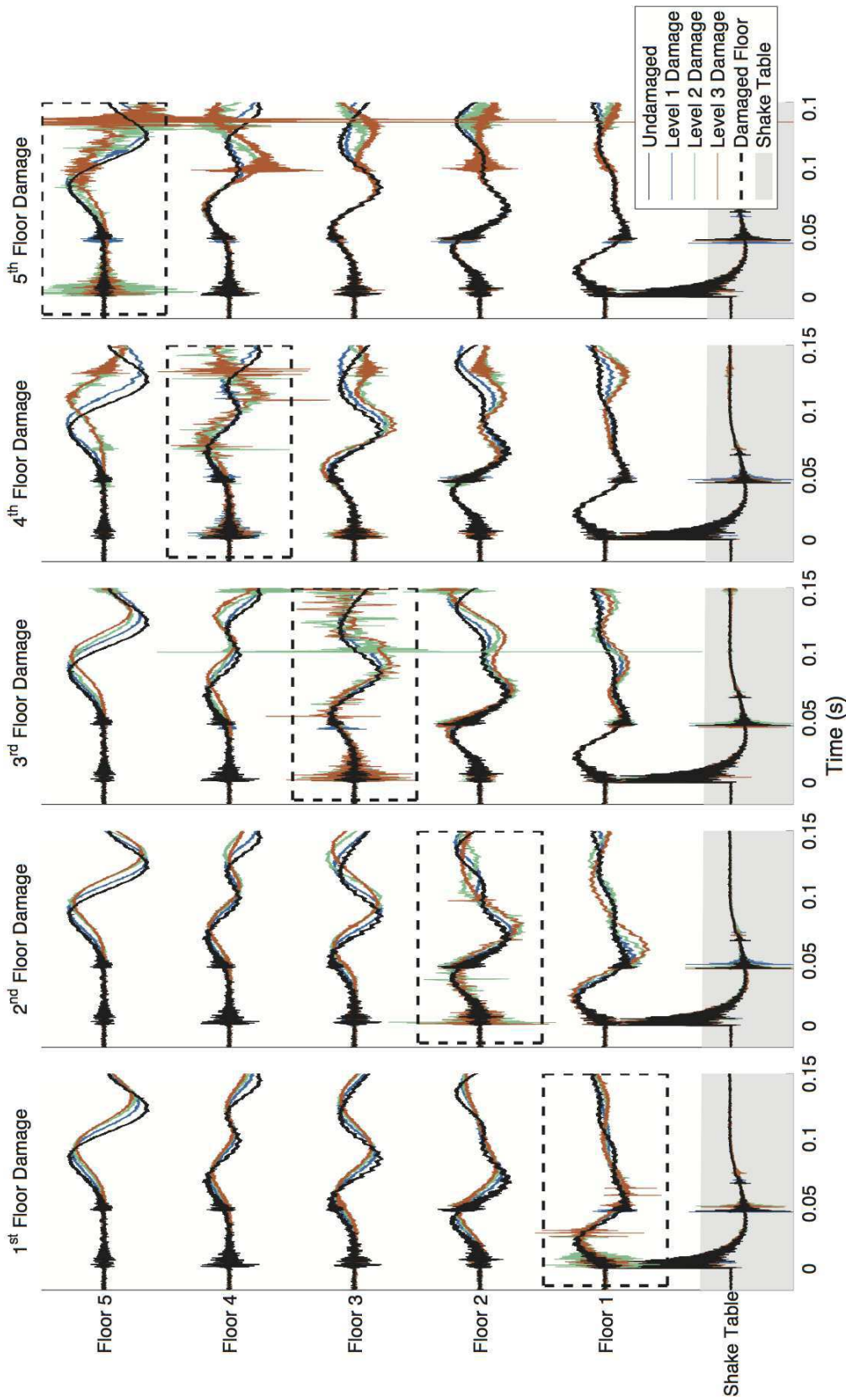


Figure 3.9: **Raw Acceleration Records: Damaged vs. Undamaged.** Features in both the low-frequency response of the structure and the high-frequency response of the structure are indicative of damage. A delay in arrival time occurs as the low-frequency shear wave propagates through the damaged region, and a reflected wave generated at the damage interface results in a slightly higher amplitude recorded below the damaged floor. The high-frequency pulse generated by the initial motion of the shake table is observed within this undamaged floor, where mechanical vibrations of the loose connections also result in large high-frequency accelerations. Additional short-duration high-frequency pulses are recorded as the structure continues to deform.

structure is indicative of damage. Much like a vertical SH wave traveling through a low velocity layer, the shear wave that propagates through the structure is slowed down when it passes through the region of damage, which consists of the damaged floor and the columns immediately above and below that floor. The low velocity zone results in increasing delays in arrival times for increasing levels of damage in records obtained above the damaged floor. A reflected wave is generated at the interface between the undamaged frame and the damaged frame, which results in slightly larger amplitudes in the shear wave pulse at the floor just below the damaged interface.

According to Timoshenko, a body's reaction to a suddenly applied force is not present at all parts of the body at once. The remote portions of the body remain unaffected during early times. Deformation propagates through the body in the form of elastic waves (Timoshenko, 1951). This concept can be applied to elastic waves that travel through the damaged region. The response of the damaged frame does not begin to differ from the response of the undamaged frame until elastic waves have had time to propagate through the damaged region and reach the location of a receiver. In this sense, there is some amount of time that passes before information of damage has been disseminated throughout the medium.

The high-frequency response of the structure is also highly indicative of damage. The initial pulse of the shake table generates a high-frequency pulse across all five floors in addition to exciting the predominant modal response of the structure. In the damaged frame, it appears that there is a decreased transmission of this high frequency energy from the damaged floor to the above floors. The energy appears to essentially become trapped at the level of the damaged floor, where the excitation of the loose connections generates mechanical vibrations that result in short-duration high-frequency accelerations (pulses) recorded on the damaged floor. As the structure continues to deform in free vibration, additional pulses are recorded. These pulses occur more often as the level of damage progresses.

Using the uniform shear beam model outlined in the Appendix, the arrival time delays (plotted in Figure 3.10) are estimated from the low-pass filtered data shown in Figure 3.20. The ratio of inter-story lateral stiffness,  $k_{damaged}/k_{undamaged}$ , is calculated as the ratio of the squares of the computed inter-story shear wave speeds,  $\beta_{damaged}^2/\beta_{undamaged}^2$ . The mean

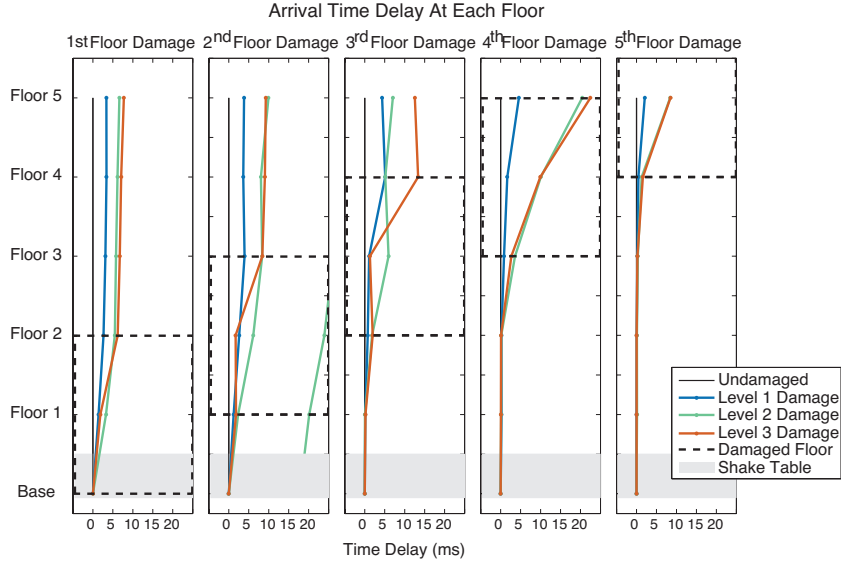


Figure 3.10: **Arrival Time Delays: Damaged Frame.** The arrival time delays are estimated from the low-pass filtered data, and are calculated relative to the arrival times obtained for the undamaged frame. Little to no change in arrival times is observed for floors below the damaged region. An increase in the arrival time delay occurs during the region of damage, and that increase in arrival time remains constant in floors above the damaged region.

values (and standard deviations) of the estimated inter-story lateral stiffness immediately beneath the damaged floor for Damage Levels 1, 2, and 3, respectively, are 0.93 (0.03), 0.70 (0.1), and 0.82 (0.23). The mean values (and standard deviations) of the estimated inter-story lateral stiffness immediately above the damaged floor for Damage Levels 1, 2, and 3, respectively, are 0.94 (0.03), 0.67 (0.09), and 0.80 (0.24). The mean values (and standard deviations) of the estimated inter-story lateral stiffness in floors not immediately above or below the damaged floor are calculated to be 0.99 (0.03), 0.95 (0.07), and 0.96 (0.05). The calculated stiffness ratios are much higher than those computed during the static testing. The estimate could be improved by taking a different approach, such as assuming a damped mass-spring model, using the shake table motion as input, and calculating the maximum likelihood estimates of model parameters that determine the best least-squares fit to the recorded floor accelerations. By using the entire time series, this approach would take much more information from the data into account in calculating the inter-story lateral stiffnesses. The amplitudes of the initial shear wave pulse (Figure 3.17) can also be used for a quick assessment of damage detection, but the presence of the transient pulses can make amplitude

estimation more difficult.

| Level of<br>Damage | Damaged<br>Floor | Lateral Stiffness between Floors |                   |                   |                   |                   |
|--------------------|------------------|----------------------------------|-------------------|-------------------|-------------------|-------------------|
|                    |                  | 0 – 1                            | 1 – 2             | 2 – 3             | 3 – 4             | 4 – 5             |
| Undamaged          | 1                | 1.00                             | 1.00              | 1.00              | 1.00              | 1.00              |
| Level 1            | 1                | 0.92 <sup>b</sup>                | 0.92 <sup>a</sup> | 0.97              | 0.98              | 1.00              |
|                    | 2                | 0.93                             | 0.91 <sup>b</sup> | 0.91 <sup>a</sup> | 1.02              | 0.99              |
|                    | 3                | 0.99                             | 0.96              | 0.98 <sup>b</sup> | 0.74 <sup>a</sup> | 1.04              |
|                    | 4                | 0.99                             | 1.00              | 0.96              | 0.95 <sup>b</sup> | 0.84 <sup>a</sup> |
|                    | 5                | 1.00                             | 1.00              | 0.99              | 0.98              | 0.91 <sup>b</sup> |
| Level 2            | 1                | 0.81 <sup>b</sup>                | 0.86 <sup>a</sup> | 0.98              | 0.98              | 0.97              |
|                    | 2                | 0.86                             | 0.77 <sup>b</sup> | 0.86 <sup>a</sup> | 1.02              | 0.89              |
|                    | 3                | 1.00                             | 0.89              | 0.73 <sup>b</sup> | 1.05 <sup>a</sup> | 0.89              |
|                    | 4                | 0.99                             | 1.00              | 0.78              | 0.58 <sup>b</sup> | 0.42 <sup>a</sup> |
|                    | 5                | 0.99                             | 1.00              | 0.99              | 0.94              | 0.60 <sup>b</sup> |
| Level 3            | 1                | 0.89 <sup>b</sup>                | 0.73 <sup>a</sup> | 0.97              | 0.98              | 0.96              |
|                    | 2                | 0.89                             | 1.01 <sup>b</sup> | 0.57 <sup>a</sup> | 0.96              | 0.99              |
|                    | 3                | 0.99                             | 0.89              | 1.04 <sup>b</sup> | 0.22 <sup>a</sup> | 1.05              |
|                    | 4                | 1.00                             | 1.00              | 0.83              | 0.53 <sup>b</sup> | 0.29 <sup>a</sup> |
|                    | 5                | 1.00                             | 1.00              | 0.99              | 0.91              | 0.61 <sup>b</sup> |

Table 3.2: **Estimated Damage Parameters from Dynamic Testing.** The ratio of inter-story lateral stiffness,  $k_{damaged}/k_{undamaged}$ , is calculated as the the ratio of the squares of the computed inter-story shear wave speeds,  $\beta_{damaged}^2/\beta_{undamaged}^2$ . A uniform shear beam model is assumed. The mean values (and standard deviations) of the estimated inter-story lateral stiffness immediately beneath the damaged floor for Damage Levels 1, 2, and 3, respectively, are 0.93 (0.03), 0.70 (0.1), and 0.82 (0.23). The mean values (and standard deviations) of the estimated inter-story lateral stiffness immediately above the damaged floor for Damage Levels 1, 2, and 3, respectively, are 0.94 (0.03), 0.67 (0.09), and 0.80 (0.24). The mean values (and standard deviations) of the estimated inter-story lateral stiffness in floors not immediately above or below the damaged floor are calculated to be 0.99 (0.03), 0.95 (0.07), and 0.96 (0.05).

<sup>a</sup> = Immediately above damaged floor

<sup>b</sup> = Immediately below damaged floor

### 3.3.4 Dynamic Testing:

#### Damage Detection Method Based on Pulse Identification

It has become apparent that 1) the presence of short-duration high-frequency signals (call them pulses) can be indicative of damage, 2) some types of damage result in the generation of a new high-frequency source mechanism in the structure, and 3) the response of a structure is consistent between trials when a similar source mechanism is applied at the same location. Information about repeating pulses present in the acceleration time series has potential use for damage detection. A schematic of the idea is illustrated in Figure 3.11. The basic idea is to compare pulses observed in the acceleration time series when the structure is in a potentially damaged state to pulses observed when the structure was known to be in an undamaged state. By comparing the pulses in these two situations, a change in this type of high-frequency dynamic behavior of the structure can be identified. The approximate location of the damage source can be determined from the arrival times and amplitudes of the pulses. These regions can be analyzed in the context of potential nearby sources of high-frequency excitation, including the possibility of damage. Pulses can be generated by various mechanisms related to damage, including acoustic emission generated by the propagation of a crack tip, elastic waves generated by mechanical impact of loose parts, or multi-modal traveling waves that can occur during the dynamic loading of flexible structural members such as the propagation of a flexural wave through a beam. Pulses can also be generated by environmental mechanisms, such as a car driving over a bump on a bridge, the collapse of a bookshelf during an earthquake, or an impact hammer. Hence, it is preferable to have a baseline recording to which possible damage features can be compared.

A series of dynamic tests is conducted on the shear beam in order to experimentally test this method. In Damage State A, damage is introduced to the frame by loosening a single screw. In Damage State B, the frame is further damaged by loosening a screw at a second location. A static tilt test was performed on the structure with a single screw loosened, and the resulting roof displacements due to tilt did not deviate from those recorded for the undamaged frame; the same global stiffness was recorded, and no loss in interstory stiffness

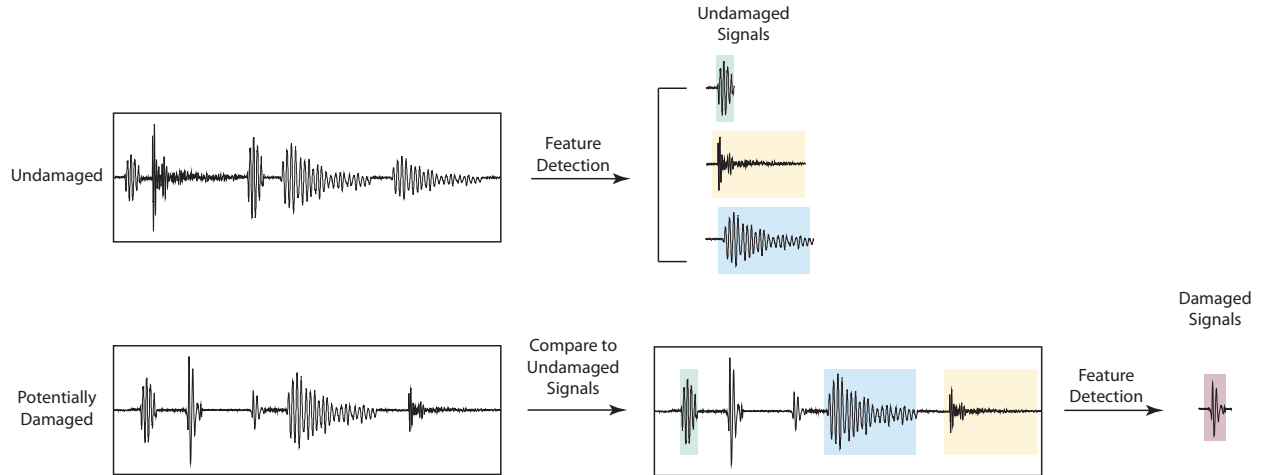


Figure 3.11: **Shear Beam: Damage Detection Method Using the Detection of Repeating Pulses.** By comparing pulses observed in the acceleration time series when the structure is in a potentially undamaged state to pulses observed when the structure was known to be in an undamaged state, changes in the dynamic behavior of the structure that could indicate damage can be identified.

was observed. The frame is subjected to a repeatable pulse at its base when it is in both an undamaged and a damaged state. The recorded accelerations, both unfiltered and high-pass filtered, are shown in Figure 3.12. The loosening of the screw allows the washer located between the head of the screw and the frame to move during loading, enough to impact the head of the bolt, on one side, or the floor column, on the other side.

In the undamaged data, shown in Figure 3.12, two distinct pulse signals are identified in the undamaged acceleration time series, and their occurrence in the time series is plotted in gray. The pulses result from the motion of the shake table, which is itself a stick-slip event of sorts. The matched filter method is applied for each identified pulse to detect its repeating presence in the high-pass filtered acceleration time series. This is done by performing a running cross-correlation that is normalized by the autocorrelation values, as given by Equations 2.1 and 2.2. Only the accelerations recorded on Floors 1-5 are used in calculating the correlation values. A threshold value of  $1/3$  is chosen, and whenever the cross-correlation value exceeds the threshold, the pulse is said to have been detected in the data. There is some art in choosing the threshold value; an increase in the probability of false negatives accompanies higher threshold values, and a decrease in the probability of false positives accompanies lower threshold values. The first identified signal,  $T_1^{UD}$ , occurs twice

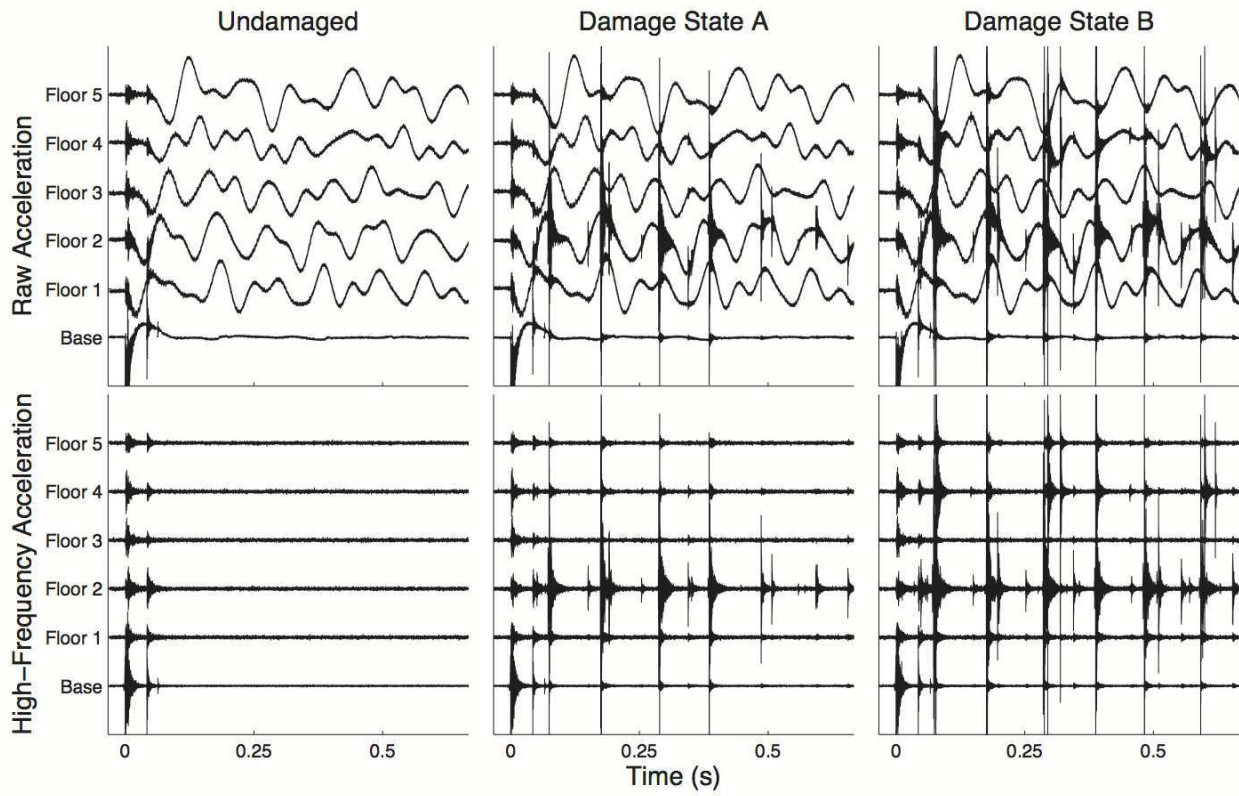


Figure 3.12: **Shear Beam: Raw and High-Frequency Accelerations.** The unfiltered and high-pass filtered (Butterworth filter, 4th order, 250 Hz) are shown above for the undamaged frame, frame with one loosened screw (Damage State A), frame with two loosened screws (Damage State B). The motion of the shake table results in a transient pulse present across all five floors. Damage results in the presence of many high-frequency pulses. The relative amplitudes have been preserved.

in the data set. The second identified signal,  $T_2^{UD}$ , occurs three times, two times during which it is embedded in  $T_1^{UD}$ .

In Damage State A, shown in Figure 3.13, the undamaged signals  $T_1^{UD}$  and  $T_2^{UD}$  are clearly identified in the data at the correct time (when the shake table supplies the initial pulse). From the remaining unidentified pulses in the Damage State A acceleration records, three damage signals,  $T_1^{DA}$ ,  $T_2^{DA}$ , and  $T_3^{DA}$  are detected. These damage signals are methodically identified. First, the first unidentified pulse that appears to consist of a single event is classified as a damage signal  $T_1^{DA}$ . Similar pulses are detected in the Damage State A acceleration records by applying the matched filter method and using a threshold value of 1/3 to identify signals in the record that have a higher correlation value. The procedure is repeated using the remaining unidentified pulses until all pulses have been classified. The damage signal templates were formed using only one of the pulses, but averaging the template over the detected occurrences could improve the signal-to-noise ratio of the damage signal. The final set of three identified damage signals is used to screen the undamaged data. This is done to determine whether one of the damage signals is present in the undamaged data set, which would suggest that it be reclassified as an undamaged signal. Damage signals  $T_1^{DA}$ ,  $T_2^{DA}$ , and  $T_3^{DA}$  are not detected in the undamaged data.

The identified damage signals all have the largest amplitudes and first arrival times on the Floor 2, and damage can be concluded to have originated at this floor. Damage was, in fact, introduced to this floor, to a screw on the opposite side of the accelerometers. An interesting phenomenon is observed by noting trends in the Floor 2 raw acceleration record when damage signals  $T_1^{DA}$  (yellow) and  $T_3^{DA}$  (blue) occur.  $T_1^{DA}$  (yellow) only occurs near the local maxima in the Floor 2 acceleration records, when the second floor is at its minimum displacement along the axis of shaking and is changing direction.  $T_3^{DA}$  (blue) only occurs after the local minima in the Floor 2 acceleration records, when the floor is at a maximum displacement and is beginning to change directions. Hence, two different signals are generated by two mechanisms resulting from the same source, namely the impact of the washer against either the head of the bolt or the side of the column. The damage events are nonlinear and aperiodic in nature. As the second damage signal  $T_2^{DA}$  only occurs once and has a similar

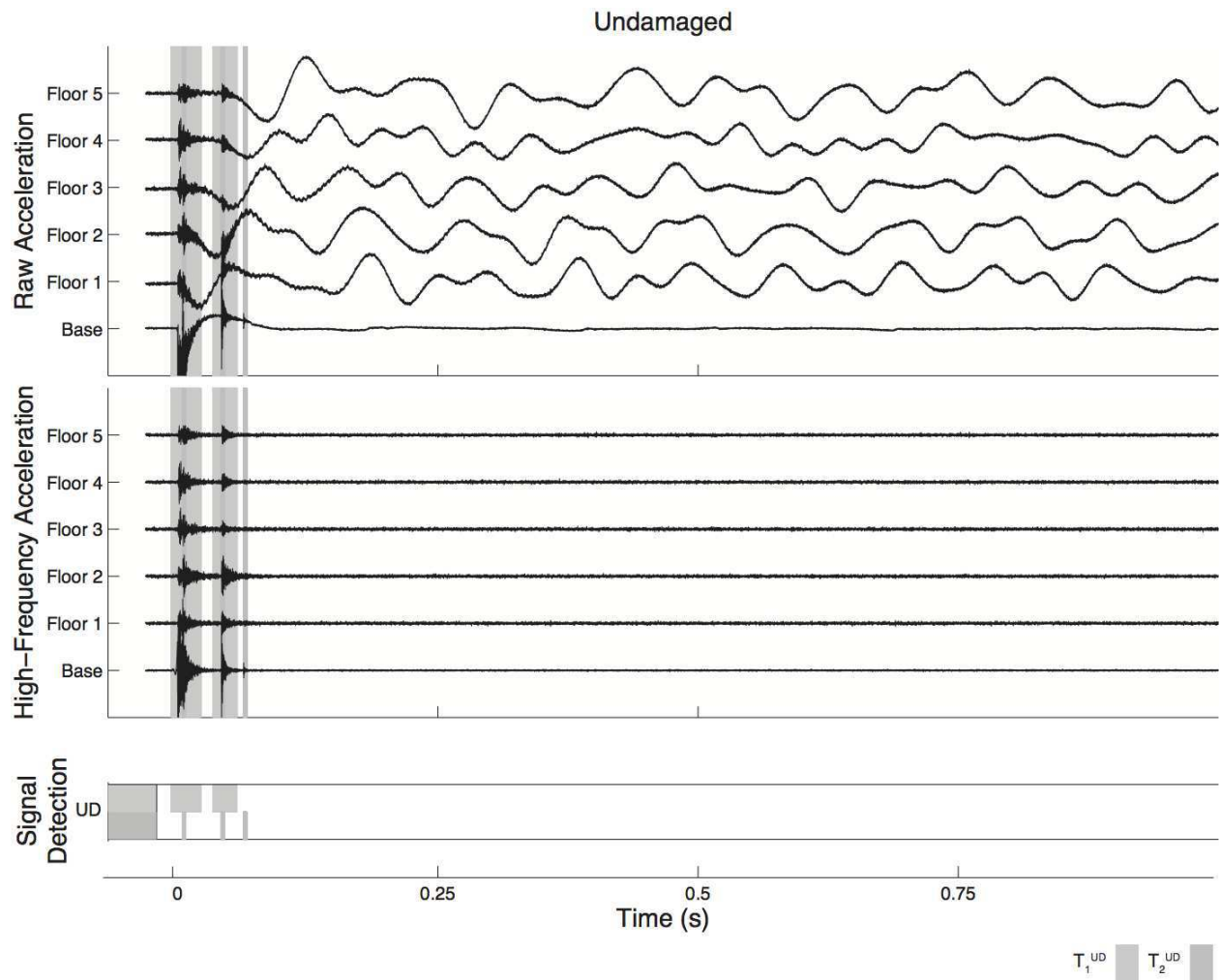


Figure 3.13: **Acceleration Pulses: Undamage Signals.** Two different pulse signals are identified in the undamaged acceleration time series, and their occurrence in the time series is plotted in gray. The pulses are due to the input pulse supplied by the shake table. A threshold value of  $1/3$  is chosen, and only Floors 1-5 are used in the analysis. The first identified signal,  $T_1^{UD}$ , occurs twice in the data set. The second identified signal,  $T_2^{UD}$ , occurs three times, two times during which it is embedded in the first identified signal.

waveform and time of occurrence to  $T_3^{DA}$ , it is likely that the second and third identified damage signals are generated by the same mechanism.

A second screw is loosened in Damage State B, and the acceleration records are plotted in Figure 3.15. Again, the initial pulse of the shake table is identified using the prerecorded undamaged signals  $T_1^{UD}$  and  $T_2^{UD}$ . Two of the Damage State A damage signals are also detected. From the remaining unidentified pulses in Damage State B, three different damage signals are detected,  $T_1^{DB}$  (yellow),  $T_2^{DB}$  (dark blue), and  $T_3^{DB}$  (red). Damage signal  $T_1^{DB}$  seems to initiate at Floor 2, and it occurs at similar points in the time history as  $T_3^{DA}$ . By looking for the presence of  $T_1^{DB}$  in the Damage State A data, we find that the damage signal  $T_1^{DB}$  is detected twice, while  $T_2^{DB}$  and  $T_3^{DB}$  are not detected. We conclude that  $T_3^{DA}$  and  $T_1^{DB}$  must be generated by the same source and mechanism. Both  $T_2^{DB}$  and  $T_3^{DB}$  originate and have the largest peak accelerations on the fourth floor. Moreover, they seem to occur at the local minima and maxima, respectively, in the Floor 4 acceleration records. Hence, we conclude that damage signals  $T_2^{DB}$  and  $T_3^{DB}$  are caused by two different mechanisms at the same source, namely a washer at Floor 4 impacting the head of the bolt or the side of the column. Damage was, in fact, introduced to this floor, to a screw on the same side as the accelerometers.

### 3.3.5 Comparison of Experimental and Theoretical Models: Undamaged Frame

There is considerable agreement between the numerical model and experimental data for the undamaged frame. A comparison of modeshapes is presented in Figure 3.16 and Table 3.3. The numerical model is computed using parameters obtained experimentally as well as parameters obtained numerically based on the material properties of aluminum and the geometry of the model. As there is much better agreement between the data and the model using the experimental parameters than there is between the data and the model using the numerical parameters, the subsequent numerical analysis is conducted using the model with the experimental parameters.

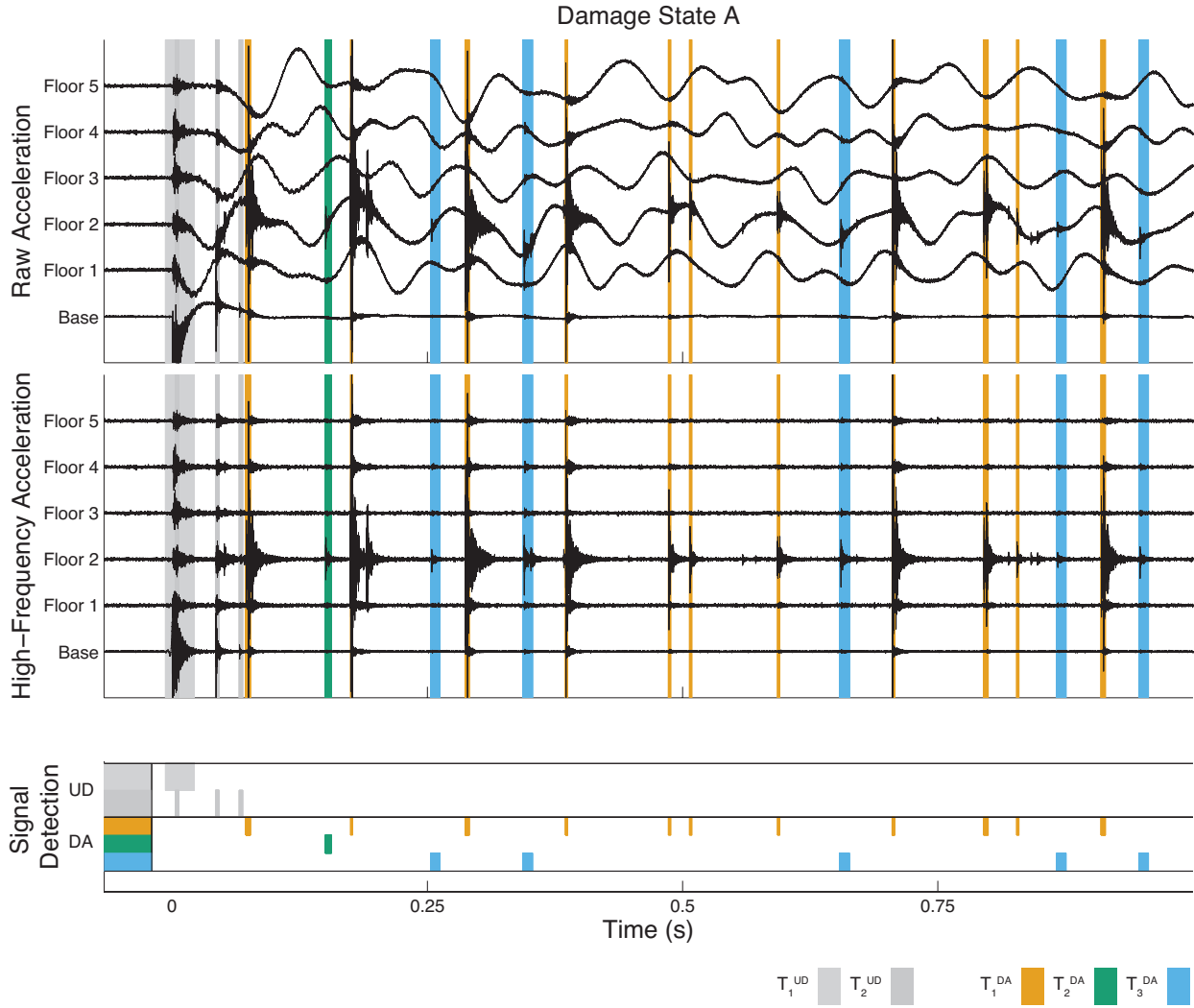


Figure 3.14: **Acceleration Pulses: Damage Signals (Damage State A)**. The pulses generated by the shake table are accurately identified using the prerecorded undamaged signals  $T_1^{UD}$  and  $T_2^{UD}$ , and their occurrence is highlighted in gray. Undamaged signal  $T_1^{UD}$  is detected once in the data set, and  $T_2^{UD}$  is detected three times, one time during which it is embedded in  $T_1^{UD}$ . Damage signals are generated by a washer between the head of the loosened screw and the frame that is able to move when the screw is loosened. Three damage signals,  $T_1^{DA}$  (orange, 11 occurrences),  $T_2^{DA}$  (green, 1 occurrence), and  $T_3^{DA}$  (blue, 5 occurrences) are detected based on the unidentified pulses. The damage signals all have the largest amplitudes and first arrival times on the Floor 2, and damage can be concluded to have originated at this floor. Damage signals  $T_1^{DA}$  and  $T_3^{DA}$  appear to be caused by different mechanisms. An interesting phenomenon is observed by noting trends in the Floor 2 raw acceleration record when damage signals  $T_1^{DA}$  (yellow) and  $T_3^{DA}$  (blue) occur. Damage signal  $T_1^{DA}$  (yellow) only occurs near the local maxima in the Floor 2 acceleration records, when the second floor is at its minimum displacement along the axis of shaking and is changing direction.  $T_3^{DA}$  (blue) only occurs after the local minima in the Floor 2 acceleration records, when the floor is at a maximum displacement and is beginning to change directions. Hence, two different signals are generated by two mechanisms resulting from the same source, namely the impact of the washer against either the head of the bolt or the side of the column. The damage events are nonlinear and aperiodic in nature. It is likely that the second and third identified damage signals are generated by the same mechanism.

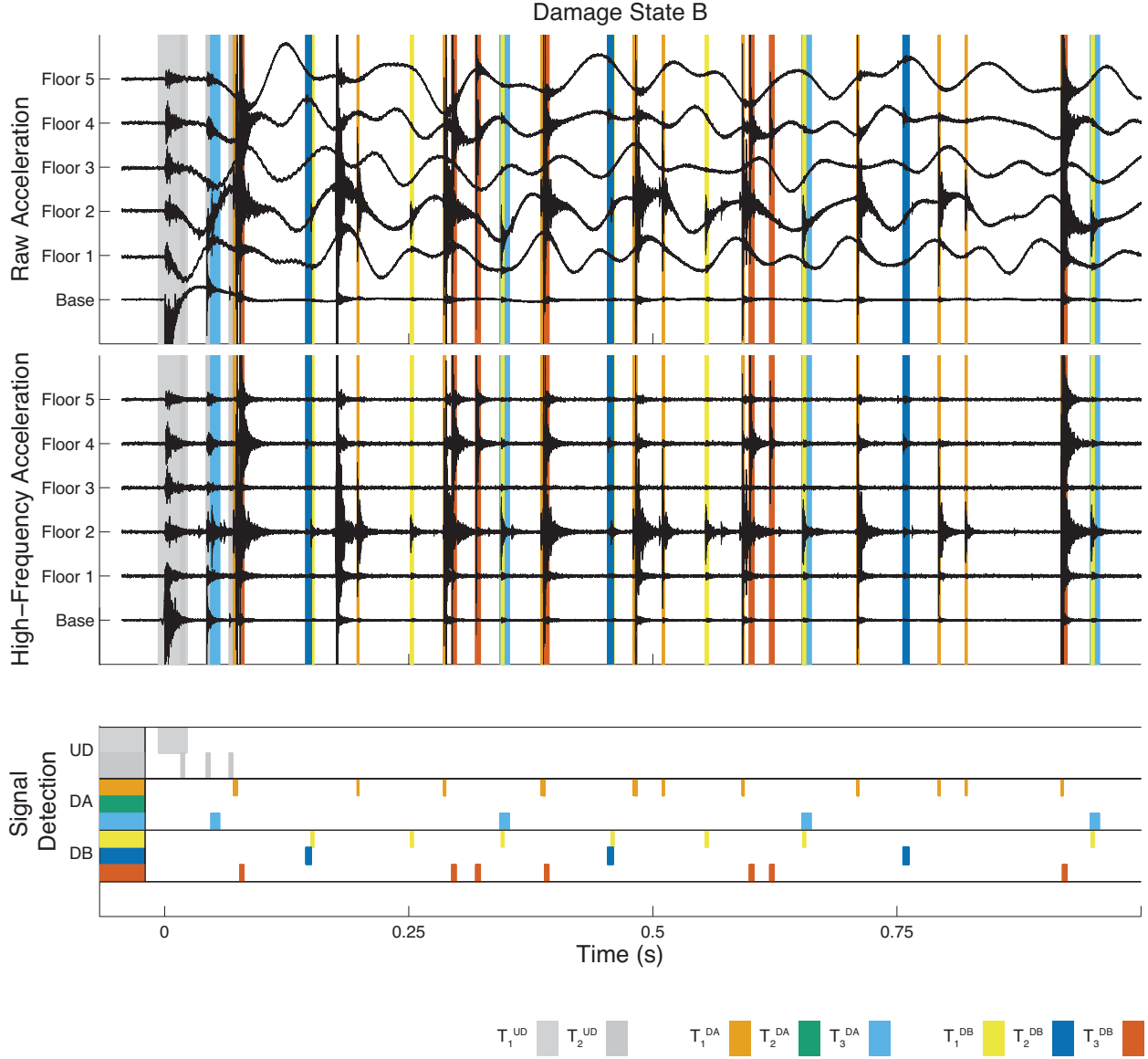


Figure 3.15: **Acceleration Pulses: Damage Signals (Damage State B)**. The initial pulse of the shake table is identified using the prerecorded undamaged signals, and the occurrence of the undamaged signals is highlighted in gray. Again, the first undamaged signal  $T_1^{UD}$  appears once in the data set, and the second undamaged signal  $T_2^{UD}$  occurs three times, one time during which it is embedded in the first signal. Two of the Damage State A damage signals are detected, with 11 detected occurrences of  $T_1^{DA}$  (orange) and four detected occurrences of  $T_3^{DA}$  (light blue). From the remaining unidentified pulses in Damage State B, three different damage signals are detected. Damage signal  $T_1^{DB}$  (yellow) occurs seven times,  $T_2^{DB}$  (dark blue) occurs three times, and  $T_3^{DB}$  (red) occurs seven times. Damage signal  $T_1^{DB}$  seems to initiate at Floor 2, and it occurs at similar points in the time history as  $T_3^{DA}$ . Hence, it is likely that this signal is caused by the same source and mechanism that causes  $T_3^{DA}$ . This is tested by looking for the presence of  $T_3^{DA}$  in the Damage State A data. In the Damage State A data, the damage signal  $T_3^{DA}$  shows up two times, while  $T_1^{DA}$  and  $T_2^{DA}$  show up zero times, and we conclude that  $T_3^{DA}$  and  $T_1^{DB}$  are generated by the same source and mechanism. Both  $T_2^{DB}$  and  $T_3^{DB}$  originate and have the largest peak accelerations on the fourth floor. Moreover, they seem to occur at the local maxima and minima in the Floor 4 acceleration records. Hence, we conclude that damage signals  $T_2^{DB}$  and  $T_3^{DB}$  are caused by two different mechanisms at the same source, namely a washer at Floor 4 impacting the head of the bolt or the side of the column.

There is considerable consistency in the response of the structure between different experimental trials. The raw acceleration waveforms recorded in three different trials are compared in Figure 3.3 for both a damaged and undamaged frame. Both the shape and amplitude of the resulting accelerations show considerable consistency for the shear wave that propagate within the structure. There is greater agreement between different trials for the undamaged frame than there is for the damaged frame. There is a seemingly stochastic occurrence of transient signals in the undamaged trial that may be due to slipping and impact between different structural members in the shear beam that lead to momentarily high accelerations.

| Mode | Observed | <u>Experimental Parameters</u> |          | <u>Numerical Parameters</u> |          |
|------|----------|--------------------------------|----------|-----------------------------|----------|
|      |          | Undamped                       | Damped   | Undamped                    | Damped   |
| 1    | 3.27 Hz  | 3.38 Hz                        | 3.38 Hz  | 2.47 Hz                     | 2.47 Hz  |
| 2    | 9.62 Hz  | 9.85 Hz                        | 9.82 Hz  | 7.20 Hz                     | 7.19 Hz  |
| 3    | 15.27 Hz | 15.52 Hz                       | 15.45 Hz | 11.36 Hz                    | 11.31 Hz |
| 4    | 19.97 Hz | 19.94 Hz                       | 19.79 Hz | 14.59 Hz                    | 14.49 Hz |
| 5    | 22.43 Hz | 21.74 Hz                       | 21.54 Hz | 16.64 Hz                    | 16.49 Hz |

Table 3.3: **Natural Frequencies of the Undamaged Shear Beam.** The ‘Observed’ natural frequencies are those experimentally observed during dynamic testing of the structure with an impulse input at the base. The theoretical natural frequencies are computed using a five-degree-of-freedom model. Both the experimentally-determined parameters (weighing the floor mass, static tilt test to determine the global stiffness value) and theoretically-determined parameters (using the geometry and material properties of aluminum) are used. Proportional modal damping is assumed, with 2% for the first mode. Good agreement is shown between the observed data and the theoretical data (using the experimentally-determined parameters).

The natural frequencies (Figure 3.18 and Table 3.4), damping values (Table 3.5), and mode shapes (Figure 3.19) for the damaged frame are obtained using the eigensystem realization algorithm (ERA) (Juang and Pappa, 1985). The ERA consists of two major parts, basic formulation of the minimum-order realization and modal parameter identification. Note that the process of constructing a state space representation from experimental data is called system realization. As expected, with increasing damage, there is a decrease in natural fre-

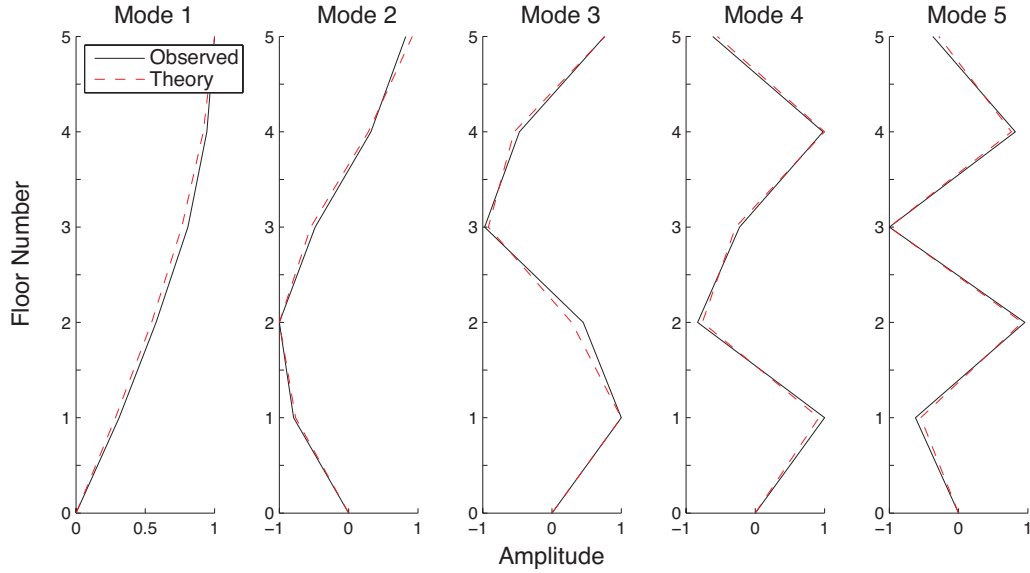


Figure 3.16: **Shear Beam: Analytical vs. Experimental Modeshapes.** There is good agreement between the observed and modeled modeshapes of the undamaged uniform shear beam. The theoretical mode shapes were computed using experimentally-obtained parameters.

quencies and and increase in damping.

### 3.4 Conclusion

The effect of damage on the dynamic response of a civil structure was investigated experimentally using a small-scale (0.75 meter tall) shear beam. Damage was introduced into the shear beam by loosening the bolts connecting the columns to the floor, and a shake table was used to apply a consistent pulse at the base of the beam. The main findings of this chapter are outlined below:

1. A dynamic pulse was input at the base of the shake table. High-frequency acceleration records could be used to immediately determine the presence and location of damage, based on the presence of short-duration high-frequency signals caused by mechanical impact and slippage. Low-frequency acceleration records could also be used to immediately determine the location of damage (i.e., which floor), based on the delayed arrival times and amplitudes of the initial shear wave.

2. A damage detection method that is based on detecting pulses in both the undamaged and potentially damaged acceleration records was found to be successful in detecting the nonlinear, aperiodic occurrences of damage signals. The arrival times and amplitudes were used to determine which floor was damaged. The advantage this strategy has over current strategies is that it can detect early onset damage. It is also based on the physical mechanism of damage in the structure, namely wave propagation, and energy formulations or the combination of the method with a time-reversed reciprocal method could give more information about the damage mechanism. The obvious disadvantage is that if there are no pulses (due to not using a high-enough sampling rate, or the absence of such a signal), the method will not work. Another disadvantage is that the method cannot be used to determine the amount of damage (e.g., loss of stiffness), it can only detect the occurrence of signals that may indicate damage. The method could be combined with a vibration-based method.
  
3. A static tilt test was performed to estimate the severity of damage for Levels 1, 2, and 3. The amount of damage was found to range from moderate to severe levels, with estimated stiffness parameter  $k_d/d_{ud}$  ranging from 0.27 to 0.74. The estimated shear wave speeds obtained during dynamic testing were used to quantify the amount of damage, and the level of damage was estimated to be less severe than the values obtained from the stiffness test. The mean values (and standard deviations) of the estimated inter-story lateral stiffnesses immediately beneath the damaged floor for Damage Levels 1, 2, and 3, respectively, were found to be 0.93 (0.03), 0.70 (0.1), and 0.82 (0.23). The mean values (and standard deviations) of the estimated inter-story lateral stiffness immediately above the damaged floor for Damage Levels 1, 2, and 3, respectively, were found to be 0.94 (0.03), 0.67 (0.09), and 0.80 (0.24). The mean values (and standard deviations) of the estimated inter-story lateral stiffness in floors not immediately above or below the damaged floor were calculated to be 0.99 (0.03), 0.95 (0.07), and 0.96 (0.05). The dynamic estimates could be improved by considering a longer portion of the time series. The values could be tested using forward modeling

| Damaged Floor | Damage Level | Mode Number |         |          |          |          |
|---------------|--------------|-------------|---------|----------|----------|----------|
|               |              | 1st         | 2nd     | 3rd      | 4th      | 5th      |
| -             | 0            | 3.25 Hz     | 9.72 Hz | 15.38 Hz | 20.10 Hz | 22.52 Hz |
| 1             | 1            | 2.77 Hz     | 9.18 Hz | 14.77 Hz | 18.79 Hz | 22.09 Hz |
|               | 2            | 2.64 Hz     | 9.04 Hz | 14.40 Hz | 18.41 Hz | 22.17 Hz |
|               | 3            | 2.59 Hz     | 9.07 Hz | 14.27 Hz | 18.50 Hz | 22.32 Hz |
| 2             | 1            | 2.86 Hz     | 9.60 Hz | 14.50 Hz | 18.95 Hz | 22.11 Hz |
|               | 2            | 2.30 Hz     | 9.49 Hz | 13.58 Hz | 18.12 Hz | 21.44 Hz |
|               | 3            | 2.30 Hz     | 9.18 Hz | 13.44 Hz | 16.74 Hz | 21.02 Hz |
| 3             | 1            | 3.09 Hz     | 9.13 Hz | 14.91 Hz | 19.64 Hz | 21.19 Hz |
|               | 2            | 2.71 Hz     | 8.28 Hz | 14.14 Hz | 19.29 Hz | 20.42 Hz |
|               | 3            | 2.50 Hz     | 7.71 Hz | 13.67 Hz | 18.63 Hz | 20.40 Hz |
| 4             | 1            | 3.11 Hz     | 8.39 Hz | 14.44 Hz | 18.29 Hz | 22.21 Hz |
|               | 2            | 2.84 Hz     | 7.12 Hz | 12.97 Hz | 16.84 Hz | 21.46 Hz |
|               | 3            | 2.79 Hz     | 6.79 Hz | 12.35 Hz | 15.58 Hz | 21.27 Hz |
| 5             | 1            | 3.25 Hz     | 9.25 Hz | 14.22 Hz | 19.00 Hz | 22.16 Hz |
|               | 2            | 3.19 Hz     | 8.22 Hz | 12.72 Hz | 18.40 Hz | 22.01 Hz |
|               | 3            | 3.16 Hz     | 7.52 Hz | 12.30 Hz | 18.26 Hz | 22.03 Hz |

Table 3.4: **Shear Beam: Observed Natural Frequencies (Damaged and Undamaged Frame).** The natural frequencies were determined using the ERA from the IRF generated by inputting a pulse at the base of the structure with a sampling rate of 1000 sps. As expected, there are considerable decreases in the natural frequencies with increasing levels of damage.

by determining the accompanying natural frequencies and mode shapes and comparing those with the observed ones.

4. The modal response of the structure was found to be highly consistent between trials, though the introduction of damage results in the presence of transient signals that generally originate at the damaged floor. A decreased transmission through the damaged floor of the high-frequency motion generated by the shake table was also observed.

| Damaged<br>Floor | Damage<br>Level | Mode Number |       |       |        |       |
|------------------|-----------------|-------------|-------|-------|--------|-------|
|                  |                 | 1st         | 2nd   | 3rd   | 4th    | 5th   |
| -                | 0               | 0.016       | 0.005 | 0.004 | 0.003  | 0.005 |
| 1                | 1               | 0.019       | 0.005 | 0.007 | 0.008  | 0.004 |
|                  | 2               | 0.019       | 0.013 | 0.009 | 0.006  | 0.015 |
|                  | 3               | 0.026       | 0.016 | 0.008 | 0.010  | 0.022 |
| 2                | 1               | 0.031       | 0.010 | 0.009 | 0.013  | 0.011 |
|                  | 2               | 0.077       | 0.026 | 0.022 | 0.022  | 0.008 |
|                  | 3               | 0.076       | 0.017 | 0.029 | 0.015  | 0.002 |
| 3                | 1               | 0.010       | 0.010 | 0.003 | 0.006  | 0.026 |
|                  | 2               | 0.025       | 0.020 | 0.007 | -0.003 | 0.010 |
|                  | 3               | 0.018       | 0.028 | 0.018 | 0.010  | 0.012 |
| 4                | 1               | 0.019       | 0.017 | 0.004 | 0.015  | 0.015 |
|                  | 2               | 0.025       | 0.023 | 0.022 | 0.020  | 0.003 |
|                  | 3               | 0.028       | 0.027 | 0.028 | 0.034  | 0.004 |
| 5                | 1               | 0.017       | 0.010 | 0.010 | 0.001  | 0.006 |
|                  | 2               | 0.015       | 0.025 | 0.015 | 0.003  | 0.002 |
|                  | 3               | 0.032       | 0.034 | 0.022 | 0.004  | 0.006 |

Table 3.5: **Shear Beam: Observed Modal Damping Ratios (Damaged and Undamaged Frame).** The modal damping ratios were computed using ERA from the IRF generated by inputting a pulse at the base of the structure with a sampling rate of 1000 sps. As expected, there are considerable increases in the damping ratios, though the structure is very lightly damped.

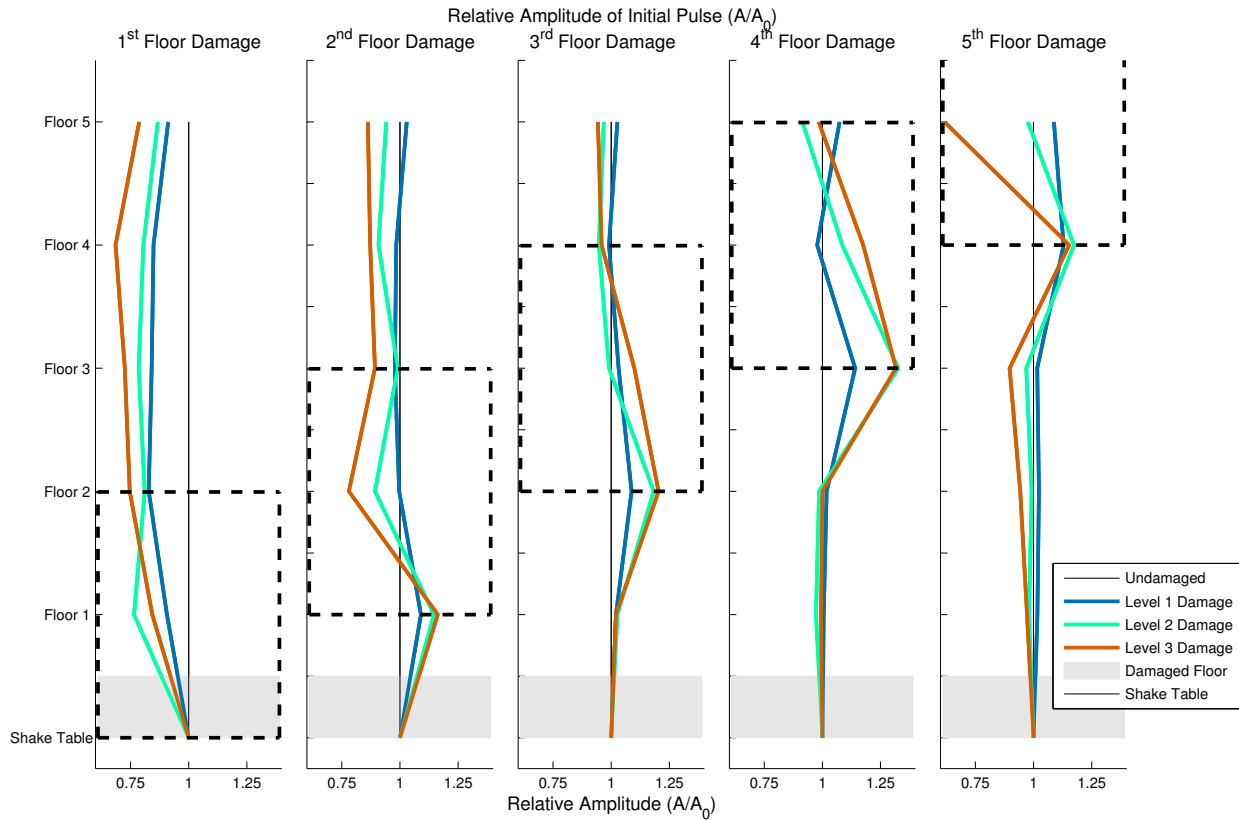


Figure 3.17: **Amplitude of Initial Shear Wave Pulse.** The amplitude of the initial shear wave pulse can be an immediate indicator of loss of stiffness, though it can be difficult to measure due to the presence of the transient signals. The amplitude is estimated from data recorded at 150 ksp/s.

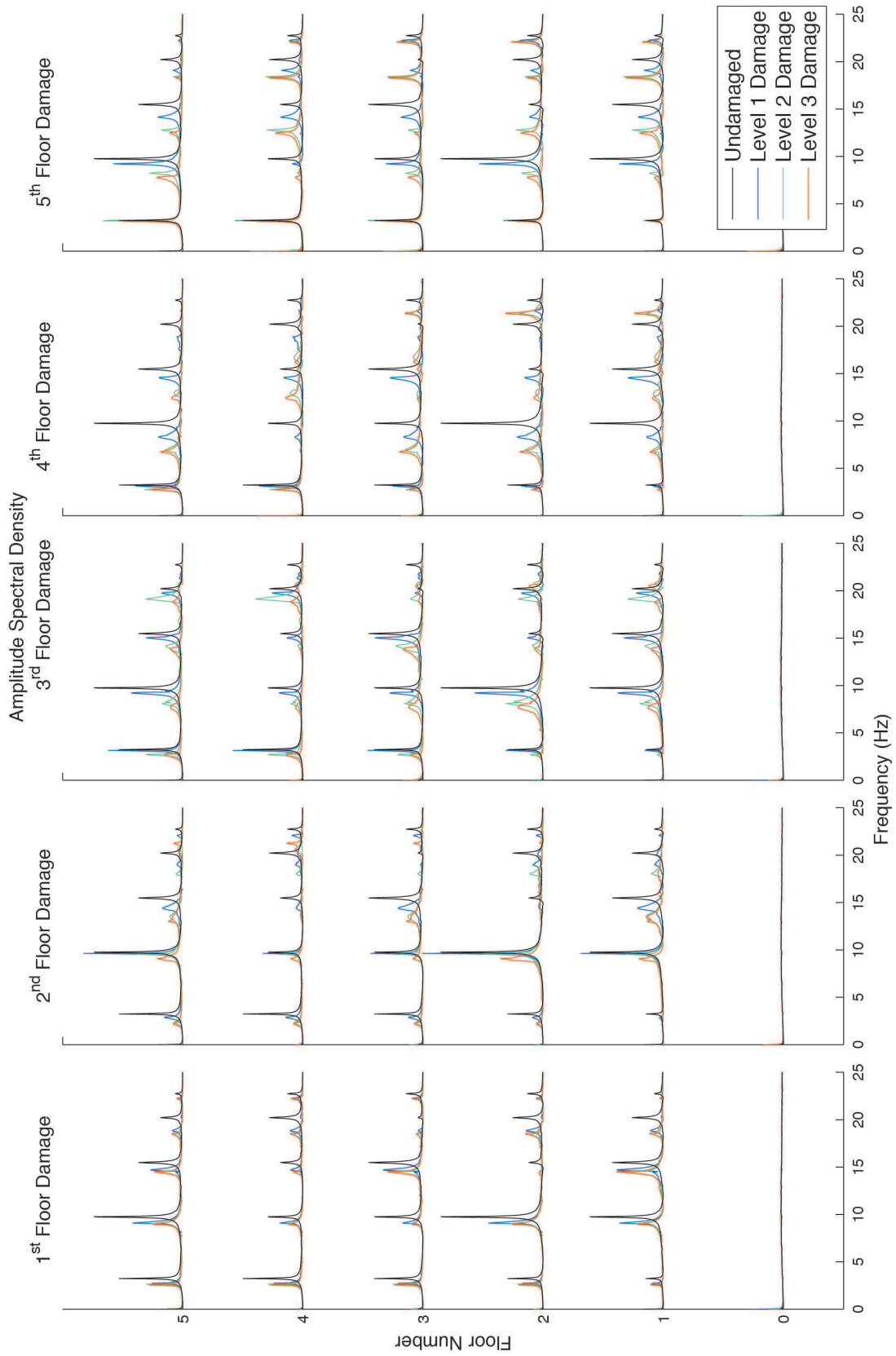


Figure 3.18: Experimental Shear Beam: Frequency Response Function. Recorded at 1 ksp/s.

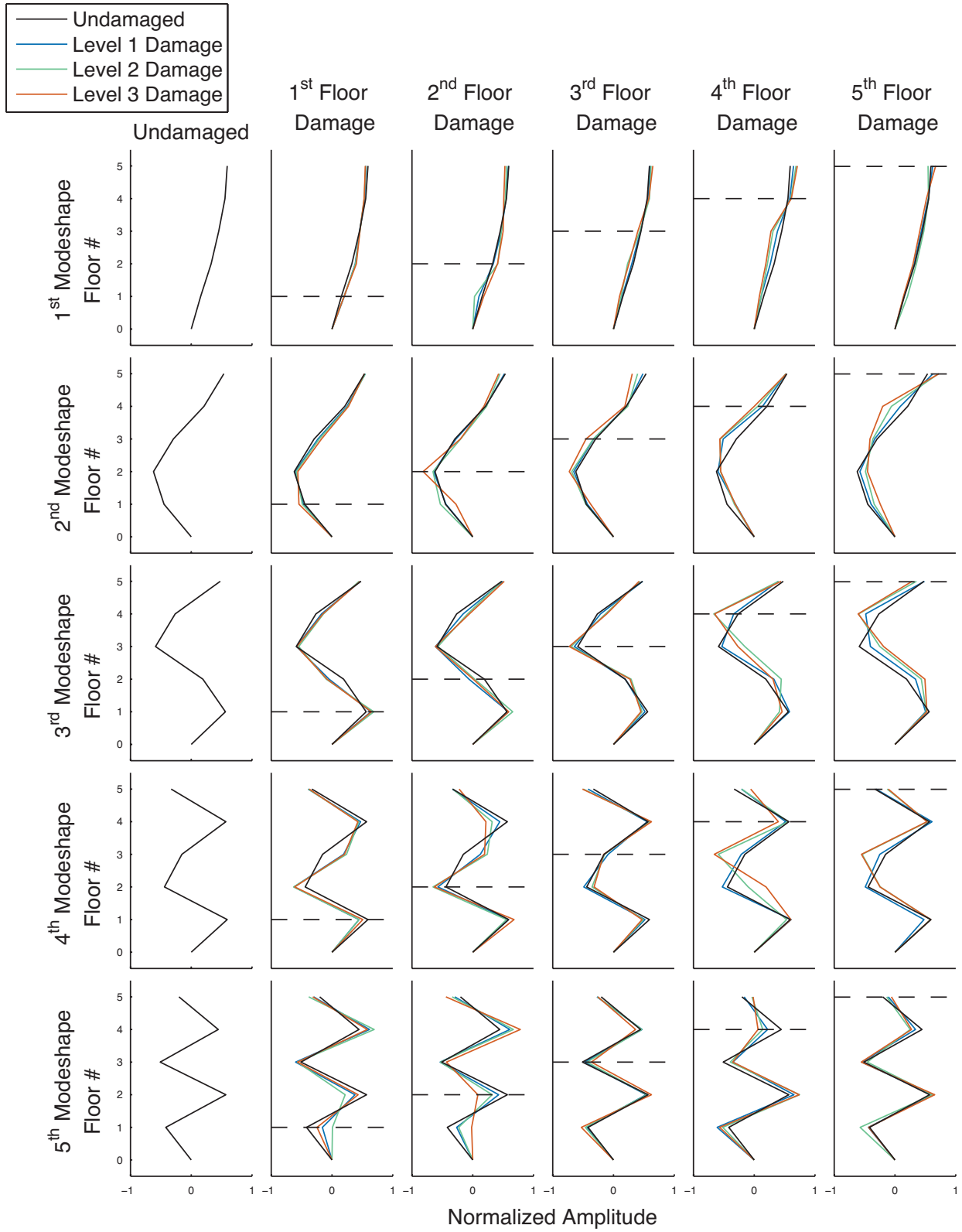


Figure 3.19: **Experimental Shear Beam: Modeshapes (Damaged and Undamaged).** Experimental modeshapes of the undamaged uniform shear beam.

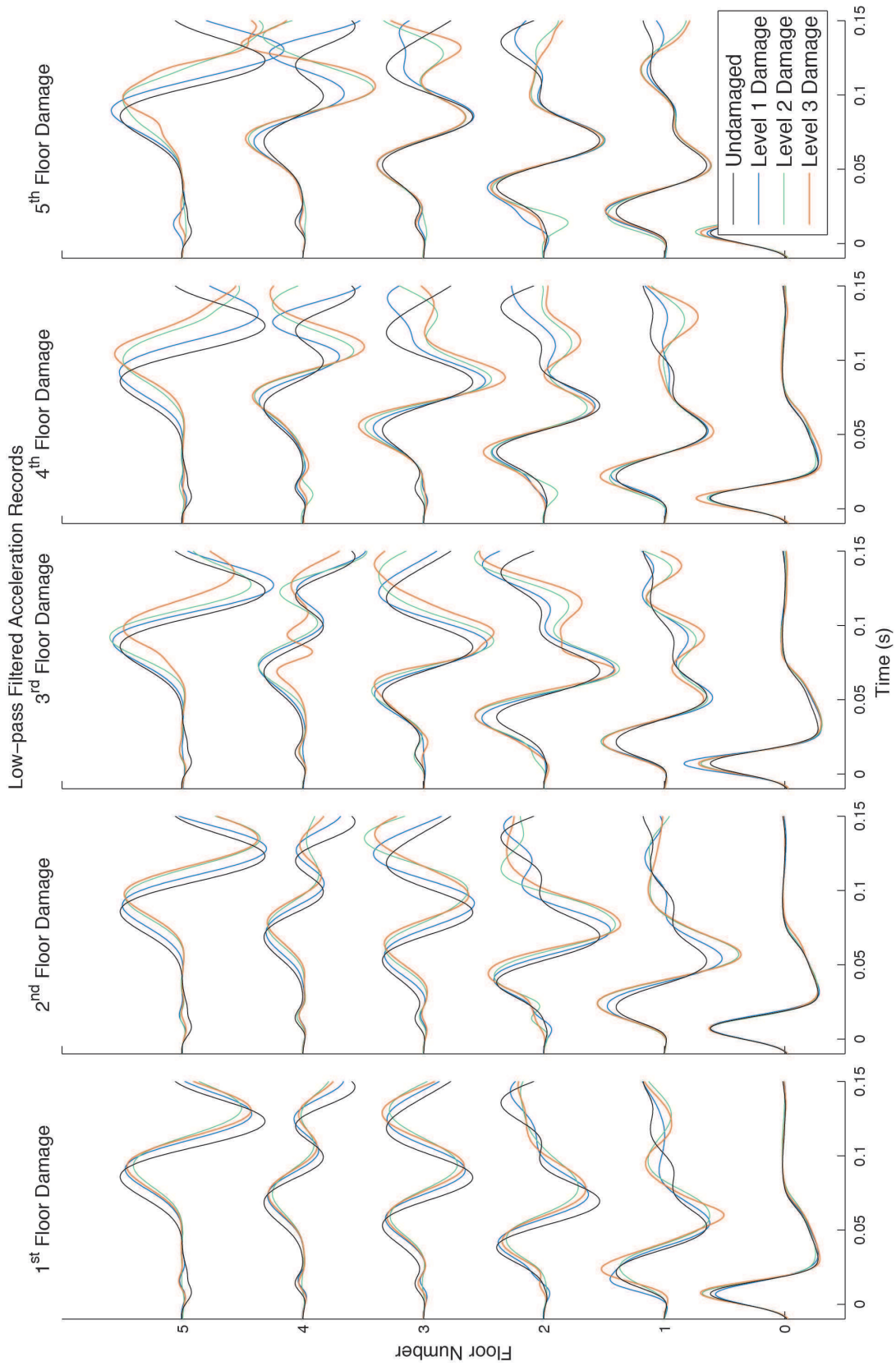


Figure 3.20: Low-Frequency Component of Accelerations. Recorded at 1 ksps.

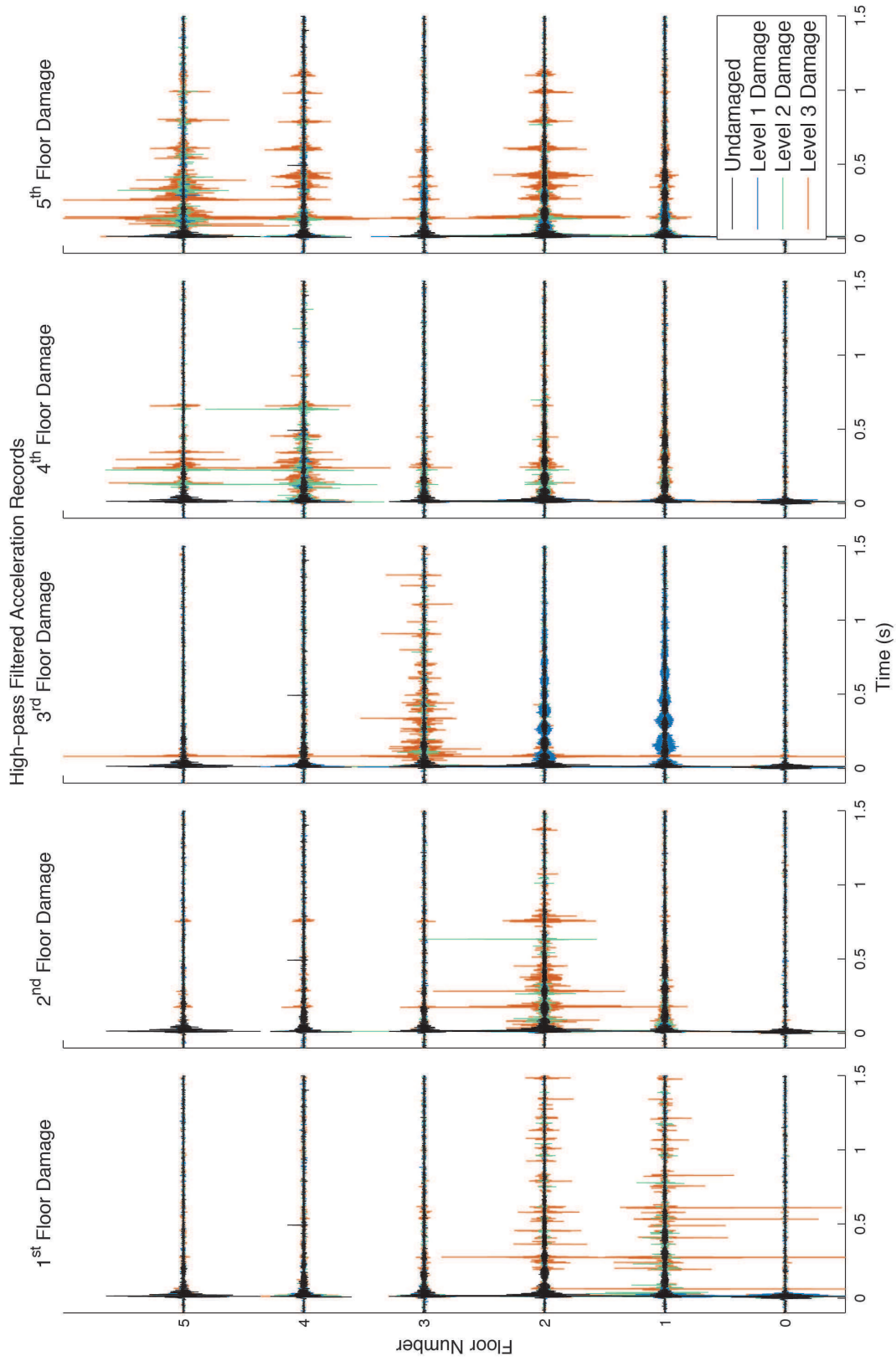


Figure 3.21: High-Frequency Component of Accelerations. Recorded at 1 ksps.